

RESEARCH ARTICLE

Human Mitochondrial Hsp70 (Mortalin): Shedding Light on ATPase Activity, Interaction with Adenosine Nucleotides, Solution Structure and Domain Organization

Paulo R. Dores-Silva¹, Leandro R. S. Barbosa², Carlos H. I. Ramos³, Júlio C. Borges^{1*}

1 Institute of Chemistry of Sao Carlos, University of Sao Paulo, Sao Carlos, SP, P.O. Box 780, 13560–970, Brazil, **2** Institute of Physics, University of Sao Paulo, Sao Paulo, SP, 05508–090, Brazil, **3** Institute of Chemistry, University of Campinas—UNICAMP, P.O. Box 6154, 13083–970, Campinas, SP, Brazil

* borgesjc@iqsc.usp.br



OPEN ACCESS

Citation: Dores-Silva PR, Barbosa LRS, Ramos CHI, Borges JC (2015) Human Mitochondrial Hsp70 (Mortalin): Shedding Light on ATPase Activity, Interaction with Adenosine Nucleotides, Solution Structure and Domain Organization. PLoS ONE 10(1): e0117170. doi:10.1371/journal.pone.0117170

Academic Editor: Harm H Kampinga, UMCG, NETHERLANDS

Received: September 6, 2014

Accepted: December 19, 2014

Published: January 23, 2015

Copyright: © 2015 Dores-Silva et al. This is an open access article distributed under the terms of the [Creative Commons Attribution License](http://creativecommons.org/licenses/by/4.0/), which permits unrestricted use, distribution, and reproduction in any medium, provided the original author and source are credited.

Data Availability Statement: All relevant data are within the paper.

Funding: This work was supported by 2011/23110-0 (JCB); 2012/50161-8, Fundação de Amparo a Pesquisa do Estado de São Paulo (<http://www.fapesp.br/>) (CHIR); and 471415/2013-8—Conselho Nacional de Desenvolvimento Científico e Tecnológico (<http://www.cnpq.br/>) (JCB). The funders had no role in study design, data collection and analysis, decision to publish, or preparation of the manuscript.

Abstract

The human mitochondrial Hsp70, also called mortalin, is of considerable importance for mitochondria biogenesis and the correct functioning of the cell machinery. In the mitochondrial matrix, mortalin acts in the importing and folding process of nucleus-encoded proteins. The *in vivo* deregulation of mortalin expression and/or function has been correlated with age-related diseases and certain cancers due to its interaction with the p53 protein. In spite of its critical biological roles, structural and functional studies on mortalin are limited by its insoluble recombinant production. This study provides the first report of the production of folded and soluble recombinant mortalin when co-expressed with the human Hsp70-escort protein 1, but it is still likely prone to self-association. The monomeric fraction of mortalin presented a slightly elongated shape and basal ATPase activity that is higher than that of its cytoplasmic counterpart Hsp70-1A, suggesting that it was obtained in the functional state. Through small angle X-ray scattering, we assessed the low-resolution structural model of monomeric mortalin that is characterized by an elongated shape. This model adequately accommodated high resolution structures of Hsp70 domains indicating its quality. We also observed that mortalin interacts with adenosine nucleotides with high affinity. Thermally induced unfolding experiments indicated that mortalin is formed by at least two domains and that the transition is sensitive to the presence of adenosine nucleotides and that this process is dependent on the presence of Mg²⁺ ions. Interestingly, the thermal-induced unfolding assays of mortalin suggested the presence of an aggregation/association event, which was not observed for human Hsp70-1A, and this finding may explain its natural tendency for *in vivo* aggregation. Our study may contribute to the structural understanding of mortalin as well as to contribute for its recombinant production for antitumor compound screenings.

Competing Interests: The authors have declared that no competing interests exist.

Introduction

Human mortalin (also named mtHsp70, GRP75, HspA9 and PBP74) [1–4] is a highly conserved molecular chaperone of the Hsp70 family that is primarily found in the mitochondria. Depending on its localization and its binding partners, mortalin has been associated with several functions, such as anti-apoptosis; interaction with wild-type p53 in the cytoplasm reducing its transcriptional activity [5–7]; transportation of nucleus-encoded proteins to the mitochondrial matrix [8–11] and to different regions of the cell [7]; cellular protection [6, 12–14]; cell protection against oxidative stress and death [13, 15–17]; and import and translocation of cytosolic proteins by association with Hsp60 [18], among other functions [4]. Moreover, mortalin is the import motor that drives the preprotein import process and helps the folding of these proteins in the mitochondrial matrix [11, 19]. Due to their importance for protein homeostasis, Hsp70 proteins have been considered targets for the drug-based treatments for cancers [7, 20–22], misfolding diseases and protein folding disorders [23].

Mortalin presents similar structural elements as other Hsp70 proteins: an N-terminal ATPase domain (NBD) and a C-terminal peptide-binding domain (PBD). These two domains should be reciprocally controlled by a bidirectional heterotrophic allostery dependent on the presence of ATP/ADP on the NBD and a client protein bound to the PBD [22, 24]. An ATP-bound state in the NBD leads the PBD to achieve a low-affinity state with client proteins, whereas peptide binding to PBD in the presence of a J-protein co-chaperone stimulates weak ATPase activity in the NBD, which leads to conformational changes in Hsp70, resulting in an enhancement of the affinity of the PDB for client proteins. The exchange of ADP for ATP in the NBD returns the PBD to a low-affinity state for client proteins, leading to its release [22]. The mammalian mitochondria also presents the main Hsp70 co-chaperones: 1) J-proteins (Hsp40), which should stimulate Hsp70 ATPase activity, and 2) two GrpE orthologous proteins, which should act as nucleotide exchange factors controlling the rate cycle of Hsp70 [22].

The mammalian mtHsp70 is also called mortalin due to its activity in the senescence and cellular death processes in rats, which present two mortalin isoforms, namely MOT1 and MOT2 [25, 26]. MOT2 has only two different amino acids in the PBD and is associated with cell immortality. Humans have only one mortalin orthologue, which is similar to MOT2 [7, 24]. Interestingly, mortalin is not exclusively a mitochondrial protein because approximately 30% is found in other cellular compartments [7, 27, 28]. It has been shown that human mortalin is involved in several cellular processes, may present important roles in Parkinson's and Alzheimer's diseases [7, 21] and is overexpressed in cancer [13, 29]. Based on these observations, there is widespread interest for the functional and structural study of mortalin and the assessment of its regulation by co-chaperones and ligands [7] because the study of this protein has been limited due to its self-aggregation when produced heterogeneously [11, 30–32]. Our search of the literature identified only one study on full-length recombinant human mortalin, which was produced in inclusion bodies and obtained through chemical refolding strategies for structural/functional characterization [33]. Nevertheless, it is well known that chemical refolding cannot be reliable for obtaining recombinant proteins with all of their structural signatures. In the case of recombinant human mortalin, the samples did not show Hsp70 signatures, and the chemical refolding approaches led to protein aggregation/precipitation [33]. A new human mitochondrial Hsp70 co-chaperone denoted Hsp70-escort protein (hHep1) was recently reported to act by preventing mortalin self-aggregation [32, 34–36]. Using a co-expression strategy with hHep1, Zhai et al. (2008) obtained recombinant human mortalin in its monomeric and active form [32], suggesting the reliability of this strategy.

To deepen the structure-function relationship of human mortalin, we obtained the recombinant protein in its soluble and functional state and compared it to human Hsp70–1A: a

cytoplasmic Hsp70 counterpart. The hydrodynamic characterization indicated that mortalin was obtained in the monomeric state, noting the effectiveness of the induction and purification protocols developed. The spectroscopy data confirmed that human mortalin was obtained with secondary and tertiary structures characteristic of homologous Hsp70. The enzyme kinetics experiments indicated that mortalin has higher ATPase activity than human Hsp70–1A. Moreover, mortalin interacted with adenosine nucleotides with a micromolar dissociation constant. The small angle X-ray scattering data noted mortalin's monomeric state in the testing conditions and allowed the generation of an *ab initio* model, indicating its slightly elongated shape. Interestingly, the thermal stability characterization showed that mortalin is composed of two domains, which are sensitive to adenosine nucleotide in the presence of Mg^{2+} ions. These experiments also indicated that mortalin undergoes aggregation/association in the first thermal-transition that was not observed during the unfolding of human Hsp70–1A, and this finding may help explain the natural tendency of the *in vivo* aggregation reported for mortalin. To the best of our knowledge, this study is the first to shed light on the structure of a functional human recombinant mortalin.

Material and Methods

Protein expression and purification

The recombinant human Hsp70–1A was expressed in the *Escherichia coli* BL21(DE3) strain as previously described [37]. The recombinant human mortalin was produced as described by Does-Silva et al. [34] with some modifications. Summarily, to obtain human mortalin in soluble form, it was co-expressed with its co-chaperone hHep1. The cells co-transformed with pET23a::hHep1 and pET28a::Mortalin were grown at 37°C in LB medium containing 50 $\mu\text{g}\cdot\text{mL}^{-1}$ ampicillin and 50 $\mu\text{g}\cdot\text{mL}^{-1}$ kanamycin to $A_{600\text{ nm}}$ of 0.7, at which point protein expression was induced by 0.2 $\text{mmol}\cdot\text{L}^{-1}$ IPTG. After 18 h of induction at 23°C, the cells were harvested by centrifugation for 20 min at 2,600 x g. For cell lysis, the pellet was resuspended in 50 $\text{mmol}\cdot\text{L}^{-1}$ Tris-HCl (pH 8.0) and 100 $\text{mmol}\cdot\text{L}^{-1}$ KCl (15 mL/200 mL of LB medium) and incubated with 5 U of DNase (Promega) and 30 $\mu\text{g}\cdot\text{mL}^{-1}$ lysozyme (Sigma) for 60 min in ice. The pellet was then disrupted through two sonication steps and then centrifuged at 20,000 x g and 4°C for 30 min. The supernatant was filtered, subjected to Ni^{2+} -affinity chromatography in 20 $\text{mmol}\cdot\text{L}^{-1}$ phosphate (pH 7.5) and 100 $\text{mmol}\cdot\text{L}^{-1}$ NaCl, and eluted in the same buffer containing 500 $\text{mmol}\cdot\text{L}^{-1}$ imidazole. Immediately after the elution, the material obtained was incubated with alkaline phosphatase (New England BioLabs) on ice for 4 h to eliminate any traces of adenosine nucleotide [37] and subjected to size exclusion chromatography with a Superdex 200 pg column (GE Healthcare Life Sciences) in TKP buffer (25 $\text{mmol}\cdot\text{L}^{-1}$ Tris-HCl, pH 7.5, 50 $\text{mmol}\cdot\text{L}^{-1}$ NaCl, 5 $\text{mmol}\cdot\text{L}^{-1}$ sodium phosphate, 5 $\text{mmol}\cdot\text{L}^{-1}$ KCl, and 2 $\text{mmol}\cdot\text{L}^{-1}$ β -mercaptoethanol) at a controlled temperature. The efficacy of the expression and purification processes was assessed by SDS-PAGE. The protein concentration was determined spectrophotometrically using the extinction coefficient calculated for mortalin under native conditions.

Spectroscopy studies

Circular dichroism measurements were performed with a J-815 spectropolarimeter (Jasco Inc.) coupled to the Peltier system PFD 425S for temperature control. Mortalin was tested in TKP buffer at final concentrations between 5 and 10 $\mu\text{mol}\cdot\text{L}^{-1}$ in a 1-nm or 0.2-mm circular path-length cuvettes. The CD spectrum of mortalin in the presence of adenosine nucleotides (200 $\mu\text{mol}\cdot\text{L}^{-1}$) and/or Mg^{2+} (200 $\mu\text{mol}\cdot\text{L}^{-1}$) were also collected. The spectra were normalized to the mean residue ellipticity ($[\Theta]$), and the protein secondary structure content was estimated using the CDNN Deconvolution program [38].

Thermal-induced unfolding was performed with a scan rate of $1^{\circ}\text{C}.\text{min}^{-1}$ at 222 nm using a 1-mm path-length cuvette. The T_m value was the temperature at the midpoint of the unfolding transition and was determined by sigmoidal fitting of the unfolding transition. The effect of adenosine nucleotides ($200\text{ }\mu\text{mol}.\text{L}^{-1}$) and/or Mg^{2+} ($200\text{ }\mu\text{mol}.\text{L}^{-1}$) on the mortalin structure was also investigated using thermal-induced unfolding followed by $\text{CD}_{222\text{ nm}}$. Both stock solutions of these ligands were prepared in TKP buffer.

The intrinsic fluorescence emission measurements were performed in an F-4500 fluorescence spectrophotometer (Hitachi) using a $10\times 2\text{-mm}$ path-length cell with mortalin ($1\text{--}2\text{ }\mu\text{mol}.\text{L}^{-1}$) in TKP buffer at room temperature. The excitation wavelength (λ) was set to 295 nm with a band-pass of 4 nm, and the fluorescence emission was measured from 310 up to 420 nm with a band-pass of 4 nm. The data were analyzed using the maximum fluorescence emission wavelength (λ_{max}) and spectral center of mass ($\langle\lambda\rangle$), as previously described [34, 37], with a wavelength between 320 and 380 nm. The effect of the temperature on the mortalin structure was also followed by fluorescence emission. The excitation λ was set to 295 nm, and the emission spectra were collected between 310 and 420 nm after 4 min of equilibration at each temperature. The data were analyzed by the $\langle\lambda\rangle$ -values as a function of the temperature.

Hydrodynamic characterization

The Superdex 200 GL 10/30 column (GE Healthcare Life Sciences) equilibrated with TKP buffer (pH 7.5) was used to perform the aSEC experiments and to determine the mortalin Stokes radius (R_s), as previously described [34]. The standard protein mixture was constituted by apo-ferritin (480 kDa/ R_s 67 Å), γ -globulin (160 kDa/ R_s 48 Å), BSA (67 kDa/ R_s 36 Å), ovalbumin (45 kDa/ R_s 29 Å), carbonic anhydrase (29 kDa/ R_s 24 Å) and cytochrome C (12 kDa/ R_s 14 Å) (Sigma-Aldrich). The frictional ratio (f/f_0) was estimated by the ratio of the experimental R_s to the radius of a sphere of the same mass [39].

Analytical ultracentrifugation experiments were performed in a Beckman Optima XL-A analytical ultracentrifuge. The sedimentation velocity experiments for mortalin were conducted at concentrations from 300 up to $580\text{ }\mu\text{g}.\text{mL}^{-1}$ in TKP buffer at 7°C and 30,000 rpm (AN-60Ti rotor), and the data acquisition was performed at 236 nm. The SedFit software (Version 12.1, [40]) was used to fit the absorbance *versus* cell radius data, which yielded a continuous $c(S)$ distribution function of the sedimentation coefficients. The frictional ratio (f/f_0) parameter acted as a regularization parameter. The standard sedimentation coefficients ($s_{20,w}$) were identified as the maximum of the peaks of the $c(S)$ curves after corrections to eliminate the interferences caused by the buffer viscosity and density and by the temperature. The SedFit software was used to estimate the $s_{20,w}$ -values because the buffer viscosity ($\eta = 1.0 \times 10^{-2}$ poise), density ($\rho = 0.99823\text{ g}.\text{mL}^{-1}$) and mortalin partial-specific volume ($V_{\text{bar}} = 0.7336\text{ mL}.\text{g}^{-1}$) were supplied by the Sednterp program. Using the $s_{20,w}$ at each protein concentration, we calculated the standard sedimentation coefficient at a protein concentration of $0\text{ mg}.\text{mL}^{-1}$ ($s_{20,w}^0$), which is an intrinsic parameter of the particle [41], through linear regression.

Isothermal titration calorimetry

The interaction of mortalin with adenosine nucleotides (ATP and ADP) was assessed by ITC using an iTC200 microcalorimeter (GE Healthcare Life Sciences). Mortalin and adenosine nucleotides, at the indicated concentrations, were prepared in TKP buffer containing $2\text{ mmol}.\text{L}^{-1}\text{ Mg}^{2+}$. Twenty-five $1.5\text{-}\mu\text{L}$ aliquots of adenosine nucleotides at concentrations from 200 to $250\text{ }\mu\text{mol}.\text{L}^{-1}$ were injected into $203.8\text{ }\mu\text{L}$ of $10\text{--}15\text{ }\mu\text{mol}.\text{L}^{-1}$ mortalin at 20°C . The apparent enthalpy change for each injection was calculated by integrating the area under the peaks of the recorded time course of the power change. The heat associated with the injectant dilution

was determined from the baseline at the end of the titration and subtracted from the data. The data were analyzed by the Microcal Origin software using the One Set of Sites curve-fitting model to calculate the apparent binding enthalpy change (ΔH_{app}), binding stoichiometry (n), and association constant (K_A). The apparent Gibbs energy (ΔG_{app}) and apparent binding entropy change (ΔS_{app}) were calculated using the following equation:

$$\Delta G_{app} = -RT \ln K_A = \Delta H_{app} - T\Delta S_{app} \quad (1)$$

SAXS experiments

Small-angle X-ray scattering experiments were performed at the Brazilian Synchrotron Light Laboratory (LNLS, Campinas-SP, Brazil) using a monochromatic X-ray beam ($\lambda = 1.488 \text{ \AA}$) of the D02A-SAXS1 beamline. The sample-to-detector distance was $\sim 1000 \text{ mm}$, which corresponds to the scattering vector range of $0.015 < q < 0.35 \text{ \AA}^{-1}$, where q is the magnitude of the q -vector defined by $q = (4\pi/\lambda)\sin\theta$ (2θ is the scattering angle). The mortalin samples were placed in a 1-mm path-length cell formed by two mica windows, and the scattering curves were recorded at 0.6 mg.mL^{-1} in TKP buffer. The samples and buffers were subjected to X-ray frames of 100 s, and the scattering curves were corrected for the detector response and scaled by the incident beam intensity and the sample's attenuation. Tests with sequential frames were employed to check for radiation damage. The corrected scattering sample was subtracted from the scattering buffer curve. All of the intensities are in the absolute scale (cm^{-1}), and this calibration was established from the scattered intensity of ultrapure water, which depends on the isothermal compressibility and on its electron density ($I(0)_{\text{water}, 293\text{K}} = 0.01632 \text{ cm}^{-1}$) [42]. The $I(0)$ value is related to the protein concentration and MM and consequently with the monodispersity of the system.

The GNOM program was used to generate the $p(r)$ curves using the experimental scattering curve. Using the $p(r)$ function, it was possible to apply the DAMMIN program [43], which uses a simulated annealing optimization routine to search for a space-filling bead model (dummy atom model) that generates the best fit to the experimental scattering curve to obtain *ab initio* models for mortalin. We are aware that *ab initio* modeling does not provide a unique solution; thus, we performed the protein shape reconstruction by averaging 20 different *ab initio* models using the DAMAVER program package [44].

The final *ab initio* model constructed for mortalin from the SAXS data after its merge using the DAMAVER package was analyzed using the HydroPro software [45] to predict the hydrodynamic properties. This analysis allowed the comparison of the predicted hydrodynamic properties of the *ab initio* model to the obtained experimental data. The HydroPro software was set up with the radius of the atomic elements of 3.1 \AA , with sigma factors of 8 and a minibead radius in the range of 4 to 2.0 \AA . The parameters of MM (70.695 kDa) and V_{bar} ($0.7357 \text{ cm}^3.\text{g}^{-1}$) were estimated from the amino acid sequence of mortalin using the Sednterp software. Parameters such as ρ and η (for standard conditions) were estimated using the Sednterp software at a temperature of 20°C .

Moreover, the experimental SAXS curve of mortalin could also be represented by a sum of two different protein conformations. In such data analysis the experimental scattering intensity is described as the weighted sum of the *E. coli* DnaK crystallographic structure bound to ATP (in the open conformation—PDB acc. n. 4B9Q [46]) and the NMR structure for *E. coli* DnaK in the ADP state (in the closed conformation—PDB acc. n. 2KHO [47]) form factors. The form factors as well as the respective weights were calculated and fitted to the experimental SAXS curve using GENFIT software [48, 49].

ATPase activity

The mortalin and Hsp70–1A ATPase activity measurements were performed spectrophotometrically using the EnzChek Phosphate Assay kit (Invitrogen), as previously shown [50]. Summarily, the method allows the quantification of the inorganic phosphate (Pi) released from ATP hydrolysis by the enzyme. Mortalin (2.50 μM) and Hsp70–1A (2.25 μM) were prepared in TKP buffer (without phosphate ions and with 2 mmol.L^{-1} Mg^{2+}) and incubated with ATP (0 to 2 mmol.L^{-1}) for 90 min at 37°C. The negative control was in the absence of the enzyme. The samples containing the Pi hydrolyzed from ATP were incubated with 0.2 U of purine nucleoside phosphorylase (PNP) and 0.2 $\mu\text{mol.L}^{-1}$ MESG, a chromogenic substrate, for 30 min at 23°C. The absorbance was measured at 360 nm. The amount of Pi released per minute (i.e., V_0 in $\mu\text{mol.L}^{-1}.\text{min}^{-1}$) was plotted against the ATP concentration (mmol.L^{-1}), and a Michaelis-Menten fitting was used (in the Origin software) to obtain the kinetic parameters. The k_{cat} was calculated by the ratio of V_{max} with the protein concentration used in the experiment. The specific activity ($\text{pmol min}^{-1}.\mu\text{g}^{-1}$) represents the amount of Pi released per time and mass of total protein. The stimulation effect of a client protein on the mortalin and Hsp70–1A ATPase activity was tested in the presence of the NR peptide (NRLLLTGY). It was pre-incubated with mortalin or Hsp70–1A in the presence of 2 mM of MgCl_2 for 15 min at room temperature prior the incubation with 1 mM ATP for 90 min at 37°C, and then the Pi released was measured as aforementioned.

Results

Recombinant human mortalin was produced in soluble form and purified until homogeneity

The recombinant human mortalin was produced in a soluble state through its co-expression with hHep1, as previously shown [34]. The purification of mortalin to the monomeric state was performed through two chromatography steps intercalated by its incubation with alkaline phosphatase to eliminate any traces of adenosine nucleotides [37]. Fig. 1A depicts the production and purification steps. The obtained mortalin was more than 95% pure and a monomeric species. For unclear reasons, the hHep1 produced by the pET23a expression vector had low yield (data not shown) [32] and was not easily detected by SDS-PAGE (Fig. 1A). However, its effect on the maintenance of human mortalin in the soluble fraction of the lysed cells was similar (data not shown) to that obtained when hHep1 was expressed by the pQE2 expression vector [34].

Fig. 1B shows a typical aSEC profile, which shows that mortalin was eluted as four main species: 1) an aggregate species eluted into the column void, 2) a possible tetrameric species, 3) a dimeric species, and 4) the main monomeric species, which is described as the Hsp70 active form [37, 51]. The fraction corresponding to the mortalin monomeric species was isolated and concentrated to 0.6–1.0 mg.mL^{-1} (8–14 $\mu\text{mol.L}^{-1}$) for biophysical/biochemical characterization. When this fraction was immediately reloaded into the aSEC column, mortalin behaved as a monodisperse monomeric species, but it self-associated or aggregated under storage conditions (>24 h) and at high protein concentrations (> 1.0 mg.mL^{-1}) (data not shown).

Human mortalin was obtained in a folded state

The secondary and tertiary structures of mortalin were investigated through CD and tryptophan fluorescence emission, respectively. Fig. 2A represents the mortalin CD spectrum corrected to $[\Theta]$ with two minima (at 208 and 222 nm) and a maxima (at 192 nm), which are characteristic of proteins containing a large portion of α -helices in their secondary structure. Using the CDNN Deconvolution program for deconvoluting the CD spectrum, we assessed the

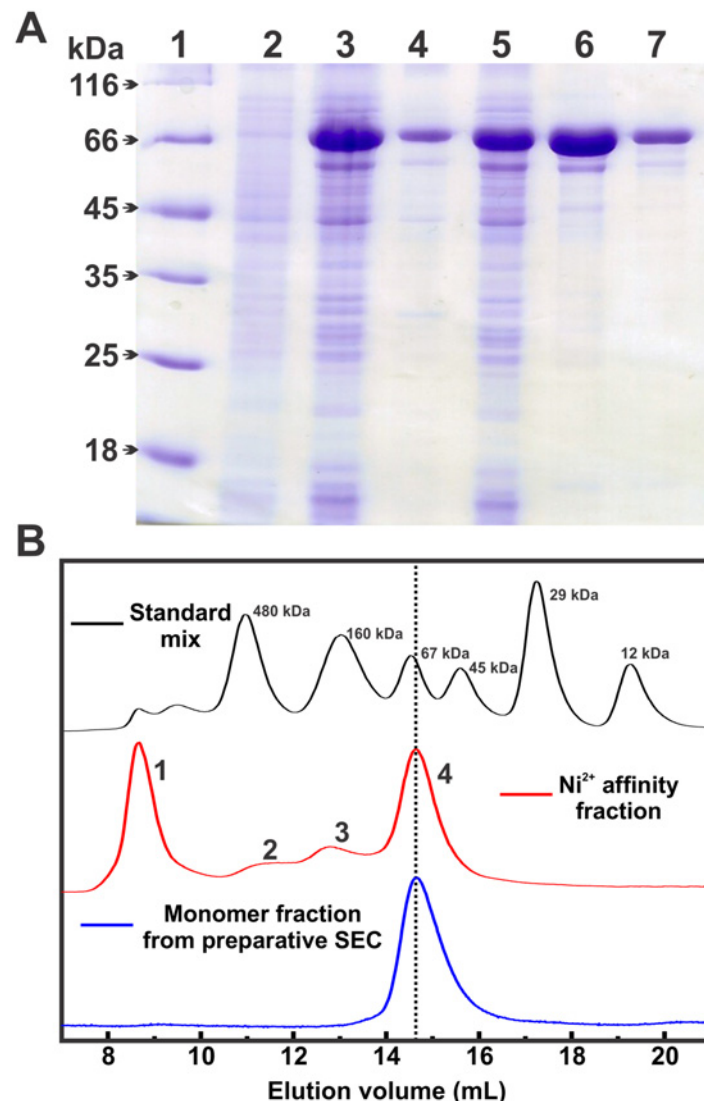


Fig 1. Mortalin production and isolation. Recombinant human mortalin (pET28a::mtHsp70) was co-expressed with recombinant hHep1 (pET23a::hHep1) in *E. coli* BL21(DE3) cells. **A)** SDS-PAGE of the produced and purified recombinant mortalin. 1) MM markers in kDa (left); 2) non-induced bacterial pellet; 3) induced bacterial pellet; 4) pellet of lysed cells; 5) supernatant of lysed cells; 6) fraction obtained from Ni^{2+} affinity chromatography; and 7) preparative SEC fraction. The final purity of mortalin was higher than 95%. **B)** aSEC profile of mortalin after Ni^{2+} affinity chromatography (red line), which showed that mortalin was eluted into four fractions (see text for details). The monomeric fraction (4) was immediately reloaded into the aSEC column and eluted as a monomer (blue line). The standard protein mixture profile is represented by the black line, and the MM of each protein is shown. The vertical dashed line marks the monomeric mortalin elution volume.

doi:10.1371/journal.pone.0117170.g001

mortalin secondary structure content as follows: 33% of α -helices, 15% of β -sheets, 18% of turns and 35% of coils (errors < 5%). Similar values were previously reported for human Hsp70-1A [37] and other Hsp70 proteins [52, 53].

Mortalin has a single tryptophan residue located in the NBD near the nucleotide-binding pocket (data not shown). Therefore, intrinsic fluorescence experiments can provide reliable information on the burial of this residue and consequently the compactness of the tertiary structure in the surrounding region. The mortalin fluorescence emissions recorded under the native

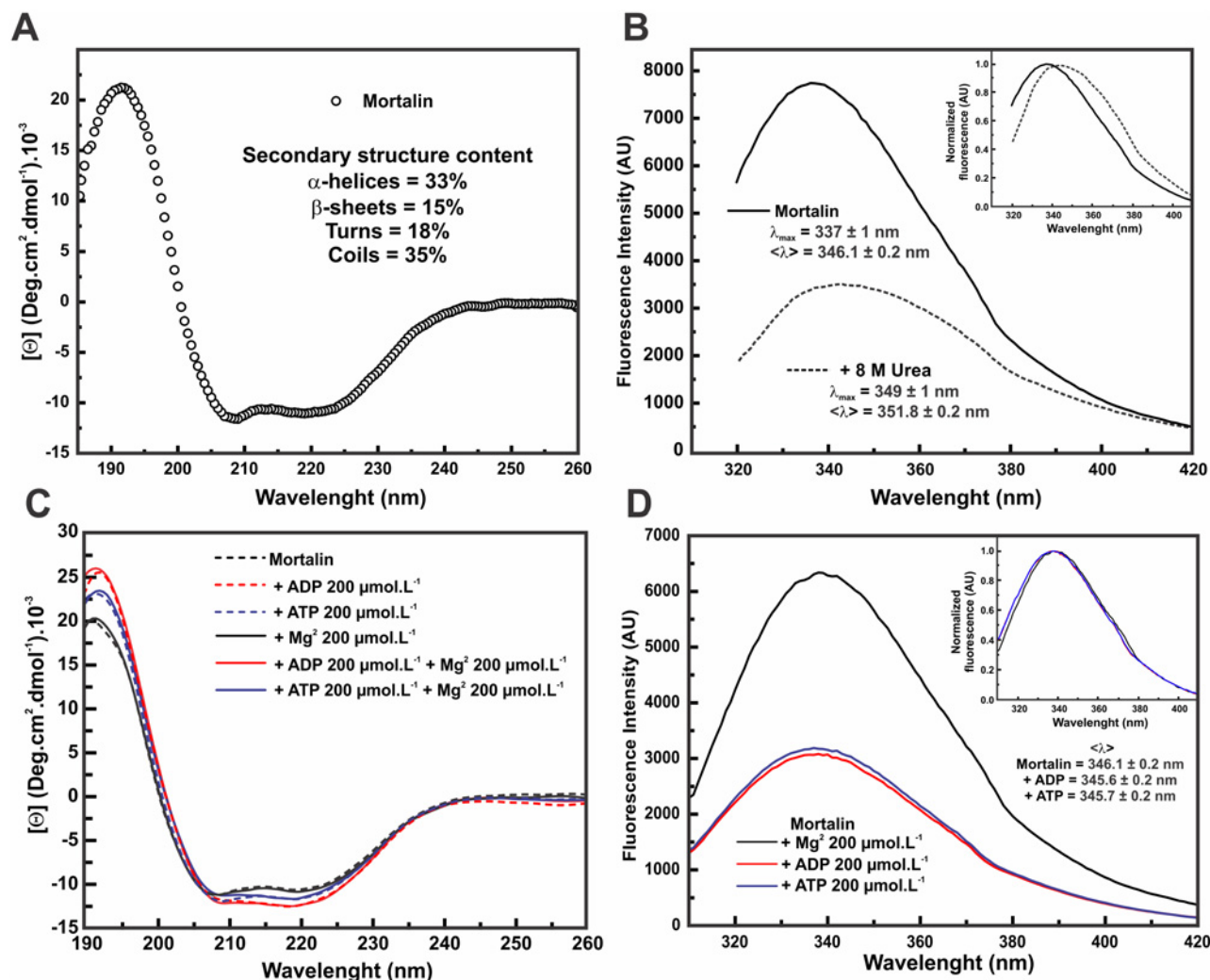


Fig 2. Mortalin was produced in its folded state. **A)** The CD spectrum shows that mortalin was obtained with a secondary structure composed of both α -helices and β -sheets. The secondary structure content, which was estimated by the CDNN deconvolution, is depicted into the figure (error < 5%). **B)** The intrinsic fluorescence emission (excitation λ at 295 nm) spectrum of mortalin had a λ_{\max} value of 337 ± 1 nm and a $\langle \lambda \rangle$ value of 346.1 ± 0.2 nm, indicating that the single Trp residue was at least partially buried. In the presence of 8 mol.L⁻¹ urea, the spectrum was quenched and suffered a red shift (λ_{\max} of 349 ± 1 nm and $\langle \lambda \rangle$ of 351.8 ± 0.2 nm), suggesting unfolding. *Inset*: normalized spectra. **C)** Mortalin CD spectra in the presence of the indicated ligands. **D)** Intrinsic fluorescence emission (excitation λ at 295 nm) spectra of mortalin in the presence of the indicated ligands, which led to a suppression of the fluorescence emission intensity and to a slightly blue shift in the spectra, as shown in the normalized fluorescence spectra (*inset*). These results suggested that mortalin was expressed in both its folded and functional state. Moreover, the presence of adenosine nucleotides and Mg²⁺ ions led to slight conformational changes in the mortalin structure.

doi:10.1371/journal.pone.0117170.g002

and chemically denaturated conditions are presented in Fig. 2B. Under the native conditions, the λ_{\max} and $\langle \lambda \rangle$ values observed were of 337 ± 1 nm and 346.1 ± 0.2 nm, respectively. In the presence of 8 mol.L⁻¹ urea, mortalin appears to unfold because the findings revealed fluorescence suppression and a spectrum red-shift (Fig. 2B, inset) in such a way that the λ_{\max} and $\langle \lambda \rangle$ values changed to 349 ± 1 nm and 351.8 ± 0.2 nm, respectively. These data suggest that the single tryptophan present in the mortalin structure is located in an environment that is partially protected from the solvent.

The effect of adenosine nucleotides (ADP or ATP) and Mg²⁺ ions was also investigated by CD and fluorescence techniques. The presence of these ligands led to slight changes in the CD

spectra (Fig. 2C) and to fluorescence emission suppression (Fig. 2D) with slight changes in the λ_{\max} and $\langle\lambda\rangle$ values (Fig. 2D, inset). Altogether, these results indicate that mortalin was obtained in the folded state and that the presence of adenosine nucleotides led to slight conformational changes in both the secondary and local tertiary structures, suggesting that these ligands interacted with mortalin.

The mortalin monomer was slightly elongated

Through hydrodynamic techniques, some conformational features of the mortalin monomeric fraction were evaluated. Using the elution volume of the mortalin depicted in Fig. 1B, it was possible to estimate its R_s through the dependence of the R_s of standard proteins and the partial coefficient k_{av} (Fig. 3A). The R_s -value determined for mortalin was 35 ± 2 Å. Using a theoretical hydrodynamic radius of 27 Å, which was calculated for a non-hydrated spherical particle with the same size as monomeric mortalin, we estimated a f/f_0 value of approximately 1.3 (Table 1), which suggests that mortalin as a monomer possesses a slightly elongated shape.

To further investigate the hydrodynamic properties of mortalin, we performed sedimentation velocity AUC experiments. Fig. 3B presents the $c(S)$ distribution function obtained for the mortalin monomeric fraction. This species behaved mainly as a monomer of 76 ± 4 kDa, with an $s_{20,w}^0$ -value of 4.8 ± 0.1 S (Fig. 3B—*inset*) under the tested conditions. The f/f_0 -value supplied by the SedFit software was 1.36 ± 0.01 (Table 1), which is in agreement with that observed by the R_s/R_0 ratio and corroborates the slightly elongated shape of the mortalin monomeric species. Both the f/f_0 - and $s_{20,w}^0$ -values are in agreement with the values reported for human cytosolic Hsp70–1A [51], suggesting their similar shapes. However, a shoulder was also observed in the $c(S)$ distribution function of mortalin, suggesting the presence of oligomeric species, which may have appeared due to the long sedimentation velocity run. The hydrodynamic data confirmed that mortalin was purified mainly in its monomeric fraction and indicated that it has a slightly elongated shape. The complementarity of the results found with different techniques is noteworthy, suggesting that artifacts are likely not present.

Mortalin has slightly higher ATPase activity than Hsp70–1A

As previously mentioned, Hsp70 presents ATPase activity mediated by NBD, which is characterized by its weakness [54]. Here, we present the ATPase activity of mortalin and Hsp70–1A in the absence of any co-chaperones. Fig. 4A depicts the ATPase activity as a function of the ATP concentration and the Michaelis-Menten fitting for both mortalin and Hsp70–1A. We can observe that mortalin exhibits slightly higher ATPase activity than Hsp70–1A, as indicated by the molecular turnover numbers (k_{cat}) of 0.151 ± 0.002 min^{−1} and 0.093 ± 0.002 min^{−1}, respectively (Table 2). Despite this finding, both proteins present a low rate of ATP hydrolysis. Table 2 presents different values for the ATPase activity available in the literature for several Hsp70s. One can observe that both mortalin and Hsp70–1A presented rates of ATP hydrolysis that were similar to those of other Hsp70s, and this fact is absolutely relevant because they indicate regulation by co-chaperones, client proteins and other ligands [22]. Specifically, the Hsp70 activity cycle is regulated by the ATP/ADP-dependent bidirectional heterotrophic allostery present on NBD and by the client protein bound to the PBD, which controls the cycle. To test if mortalin and Hsp70–1A were allosterically actives, we used the NR peptide as stimulation factor. Fig. 4B depicts the relative ATPase activity observed for mortalin and Hsp70–1A at increasing NR peptide concentrations. For mortalin, a maximum of 25% of stimulation was reached at $100 \mu\text{mol.L}^{-1}$ NR peptide indicating a half maximal effective concentration (EC_{50}) of $7 \mu\text{mol.L}^{-1}$ NR peptide. The NR peptide stimulated the Hsp70–1A ATPase activity by around 15%, which was reached at $500 \mu\text{mol.L}^{-1}$ NR peptide, resulting in EC_{50} of $170 \mu\text{mol.L}^{-1}$ NR

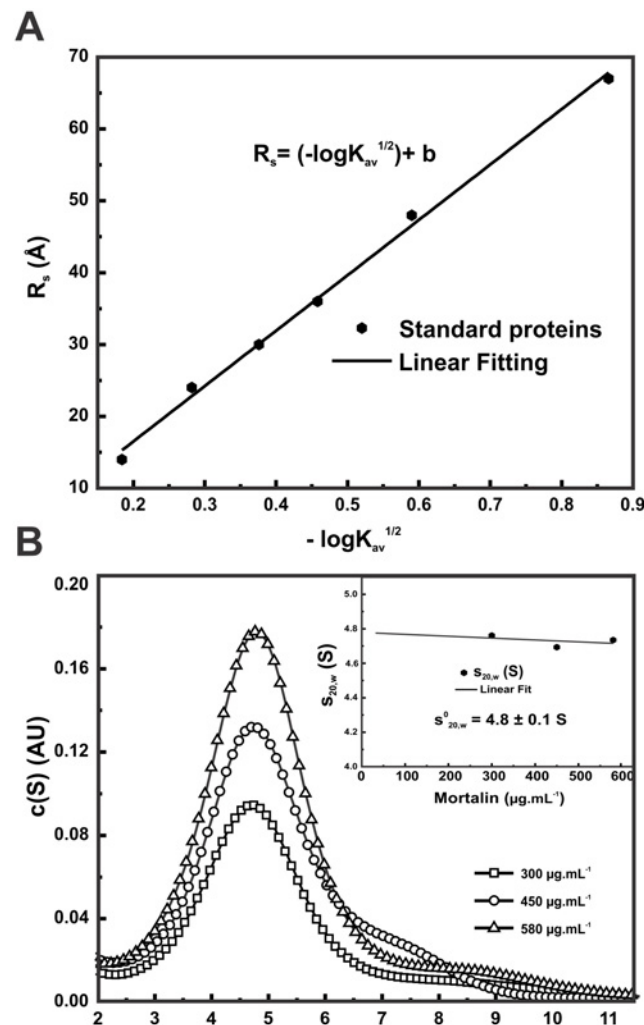


Fig 3. Monomeric mortalin was slightly elongated in solution. **A)** Estimation of the mortalin R_s based on the aSEC data presented in Fig 1B. The graph depicts the R_s of standard globular proteins as a function of the partial coefficient k_{av} , which yielded an R_s value for mortalin of $35 \pm 2 \text{ Å}$. **B)** Sedimentation velocity data resulting from the $c(S)$ distribution of mortalin, which behaved mainly as a monomeric species of $76 \pm 4 \text{ kDa}$ with f/f_0 of approximately 1.36 ± 0.01 under the tested conditions (see Materials and Methods section). *Inset:* Determination of the $s_{20,w}^0$ of mortalin through the dependence of $s_{20,w}$ on the protein concentration. Mortalin had a $s_{20,w}^0$ value of $4.8 \pm 0.1 \text{ S}$ (Table 1).

doi:10.1371/journal.pone.0117170.g003

peptide. These results indicate that both proteins were obtained allosterically active. However, the differences in the EC_{50} values and maximum stimulation indicate that mortalin and Hsp70–1A should present slightly differences in client protein specificities. In addition, this activity cycle can also be regulated by co-chaperones, such as J-domain proteins (or Hsp40), which act by speeding up ATP hydrolysis, and nucleotide exchange factors (NEFs), such as GrpE proteins [22].

Interaction studies with adenosine nucleotides by ITC

The ITC technique was used to investigate the interaction of mortalin with adenosine nucleotides. Fig 5A (upper panel) presents the results of a calorimetric titration with ADP ($\sim 250 \mu\text{mol.L}^{-1}$), which reveal an exothermic profile. The apparent heat per mol of ADP

Table 1. Summary of the hydrodynamic and structural data of mortalin.

Mortalin structural and hydrodynamic properties	Predicted for a sphere [†]		Experimental determination			
	Monomer	Dimer	aSEC	AUC [#]	SAXS	HydroPro
MM (kDa)	70.7	141.4	75 ± 4	76 ± 4	66 ± 2	-
$s_{20,w}^0$ (S)	6.1	9.6	-	4.8 ± 0.1*	-	4.9 ± 0.2
R _s (Å)	27	34	35 ± 2	-	-	34 ± 3
f/f_0	-	-	1.30 [¥]	1.36 ± 0.01	-	1.30
R _g (Å)	-	-	-	-	36 ± 2 [§] 38 ± 2 ^{&}	33 ± 2
D _{max} (Å)	-	-	-	-	130 ± 10	116 ± 3

[†] Values predicted as globular monomers in water and 20°C (predicted by the Sednterp software)

[#] calculated from SedFit from the sedimentation velocity data;

* data extrapolated for water, 20°C and 0 mg.mL⁻¹ of protein;

[§] data from Guinier law;

[&] data from p(r) curve;

[¥] data obtained using the Stokes equation for proteins of known R_s (predicted by Sednterp software).

doi:10.1371/journal.pone.0117170.t001

injected (ΔH_{app}) against the molar ratio of ADP/mortalin is depicted in the lower panel of Fig. 5A. The fitting of this curve indicated an exothermic ΔH_{app} of $-3,500 \pm 50$ cal.mol⁻¹ and a K_A value of $4.6 \pm 0.2 \times 10^5$ L.mol⁻¹, suggesting a K_D of 2.2 ± 0.1 μ mol.L⁻¹. Based on the K_A and ΔH_{app} values and Equation 1, the ΔS_{app} value was calculated to be $+13.9$ cal.mol⁻¹.deg⁻¹. The interaction of ATP with mortalin by ITC is depicted in Fig. 5B. Similarly, the fitting of the calorimetric titration of ATP into mortalin solution yielded an exothermic ΔH_{app} of $-1,500 \pm 20$ cal.mol⁻¹ and a K_A value of $9.4 \pm 0.4 \times 10^5$ L.mol⁻¹, suggesting a K_D of 1.1 ± 0.1 μ mol.L⁻¹. Using these values and Equation 1, the ΔS_{app} value was estimated to be $+22.1$ cal.mol⁻¹.deg⁻¹. These data suggested that both enthalpy and entropy drive the mortalin interaction with both adenosine nucleotides, as was also observed for human cytosolic Hsp70-1A [37]. However, the latter showed higher affinity for ADP than ATP under similar conditions [37], whereas mortalin appears to have higher affinity for ATP than ADP. The higher T_{m1} that mortalin presented in the presence of ATP-Mg²⁺ in comparison to ADP-Mg²⁺ (see below—Table 3) also indicated that this protein has higher affinity for ATP than ADP. Therefore, the ITC data suggest that mortalin interacts with both ADP and ATP with different affinities and that these interactions induce conformational changes and result in different thermodynamic signatures (ΔH_{app} and ΔS_{app}).

The stoichiometry of the interaction was approximately 0.8–0.9 for both ligands (Fig. 5), indicating a 1:1 stoichiometry because the NBD has one adenosine nucleotide-binding site. The value near 0.8 can be explained by a fraction of mortalin that is not responsive to binding ADP or ATP, likely due to the self-association process. In fact, the parallel analysis of mortalin samples at the end of the ITC experiments by aSEC showed the presence of 10–20% other species that are likely dimers (data not shown) due to the mortalin concentrations (~ 15 μ mol.L⁻¹) and the temperature used (20°C). The presence of other oligomeric species in the AUC experiments (presented here) at lower protein concentrations and experimental temperature conditions corroborate this hypothesis. When the protein concentration was corrected to simulate the mortalin monomeric fraction in the ITC sample (i.e., 80–90%), the stoichiometry reached almost 1 without causing changes in the values of the other thermodynamic parameters (data not shown). These observations noted the difficulties associated with working with mortalin in the concentrations and experimental conditions reported here and also suggested that the

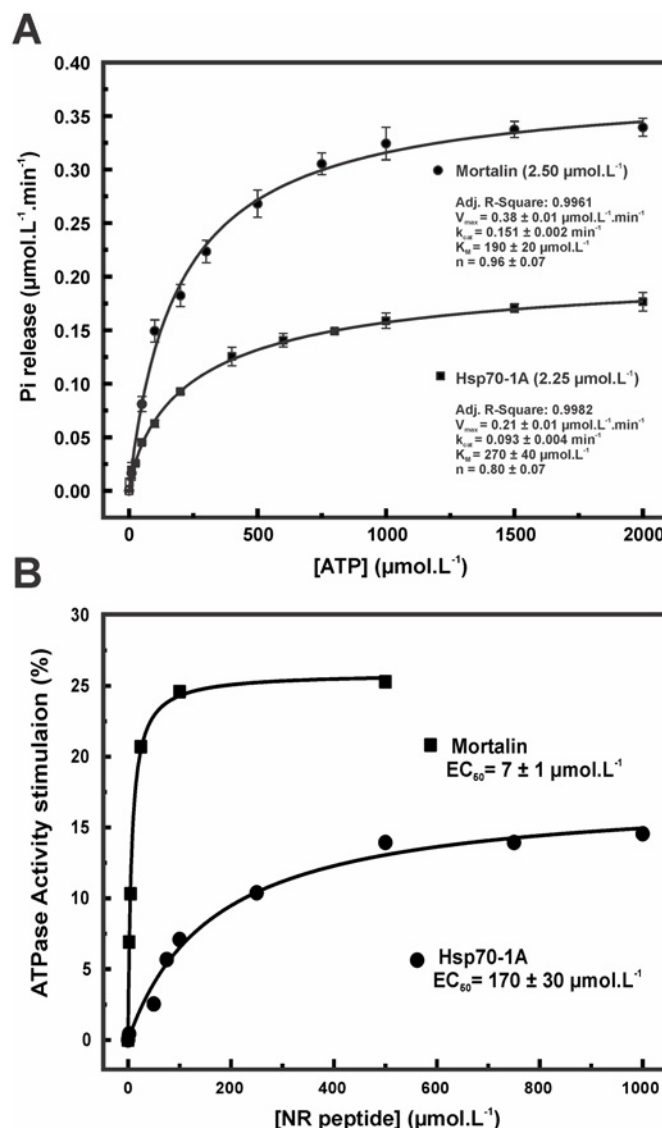


Fig 4. Mortalin has higher ATPase activity than Hsp70-1A. **A)** Mortalin (2.50 $\mu\text{mol.L}^{-1}$) and Hsp70-1A (2.25 $\mu\text{mol.L}^{-1}$) were incubated with ATP (0–2 mmol.L^{-1}) for 90 min at 37°C, and the Pi released as a result of ATP hydrolysis was quantified. The data were treated through Michaelis-Menten fitting for determination of the kinetic parameters, which are presented in the Figure and Table 2. The results suggested that both mortalin and Hsp70-1A exhibit low ATPase activity. Despite these findings, based on the k_{cat} value, mortalin presented higher ATPase activity than Hsp70-1A, although the K_{M} values of both are similar. **B)** Relative ATPase activity stimulation. Effect of the NR peptide titration on the basal ATPase activity of mortalin and Hsp70-1A at 1 mmol.L^{-1} ATP.

doi:10.1371/journal.pone.0117170.g004

other mortalin oligomeric species either did not interact with adenosine nucleotides or did interact with a lower affinity constant.

Structural analysis of mortalin by SAXS

To obtain more information on the structure of mortalin in solution, we performed SAXS experiments. It is well known that some important parameters of the proteins can be directly obtained from the scattering curve, such as the radius of gyration, R_g , and MM, using the $I(q \rightarrow 0)$

Table 2. Kinetic constants determined for human mortalin and human Hsp70–1A compared with those of homologous Hsp70.

Protein	Specific activity (pmol.min ⁻¹ .μg ⁻¹)	K _M (μmol.L ⁻¹)	k _{cat} (min ⁻¹)	Temperature (°C)	Ref.
<i>E. coli</i> DnaK	-	-	0.087 ± 0.007	37	[54]
			0.15	37	[65]
<i>E. coli</i> Hsc66	-	12.7	0.083	23	[66]
Bovine Hsc70	1.14	1.37	0.15	37	[67]
Rat Hsc70			0.12		[68]
<i>Chlamydomonas reinhardtii</i> Hsp70B	~ 9	118	-	30	[69]
Yeast Ssa	-	0.11 ± 0.04	0.031 ± 0.004	37	[70]
Yeast Ssb	-	147 ± 42	0.81 ± 0.13	37	[70]
Human Hsp70–1A	0.62 ± 0.02	270 ± 40	0.093 ± 0.002	37	[71]—This work
Human Mortalin	0.86 ± 0.02	190 ± 20	0.151 ± 0.002	37	This work

Comparing the k_{cat} to other members of Hsp70 family we notice that the values are too close of each other, Sadis & Hightower [67] found a k_{cat} of 0.15 min⁻¹ for bovine brain Hsc70, while the recombinant rat Hsc70 presented 0.12 min⁻¹ for the ATPase activity.

doi:10.1371/journal.pone.0117170.t002

of the scattering curve obtained from Guinier's law (Fig. 6A—inset). Our data indicated that the R_g and MM values calculated for mortalin were 36 ± 2 Å and 66 ± 2 kDa, respectively. These results are in agreement with a monomeric and monodisperse mortalin (Table 1).

Fig. 6A shows the experimental scattering curve of mortalin along with the best curve obtained with the GNOM software, and the respective p(r) function can be appreciated in Fig. 6B. The p(r) curve noted that mortalin has a prolate shape with a maximum dimension (D_{max}) of 130 ± 10 Å, whereas the protein R_g is 38 ± 2 Å, which is in accordance with the Guinier analysis.

Using the p(r) function, 20 independent *ab initio* models for mortalin in solution were generated. These 20 DAMMIM models were merged using the DAMAVER program, resulting in the final *ab initio* model (Fig. 7). The normalized spatial discrepancy (NSD) of the DAMMIM models was 0.7 ± 0.1, which indicated the overall quality of the generated models [55]. One should bear in mind, however, that this procedure is valid for monodisperse systems [56].

The final *ab initio* model was also subjected to HydroPro program analysis to estimate some of its hydrodynamic and structural properties (Table 1), which were close to the experimental ones. These results suggested that the proposed model based on the SAXS data analysis represents mortalin in solution. The *ab initio* model noted that mortalin has an elongated shape (Fig. 7A). Fig. 7B is the manual adjustment of the crystallographic structures of the mortalin NBD (PDB acc. no. 4KBO), obtained in apo-state [57], and PBD of the *E. coli* DnaK (PDB acc. no. 1DKX) bound to a synthetic peptide in the peptide binding site [58], into the *ab initio* model. This adjustment suggests that the *ab initio* model is suitable to accommodate both NBD and PBD of Hsp70 even considering that the model was generated from SAXS curve in apo-conditions. The full length *E. coli* DnaK crystallographic structure (PDB acc. n. 4B9Q), obtained bound to ATP and with the PDB in the open conformation [46], was used for its manual adjustment into mortalin *ab initio* model. As can be seen in Fig. 7C, in spite of the similar dimensions, the mortalin *ab initio* model did not properly adjust some portions of the crystallographic structure. This discrepancy is probably due to the protein dynamics in solution. It is noteworthy, in the SAXS point of view, the scattering curve is a weighted average of all protein conformations present in solution [56] and the *ab initio* model is a rigid representation of the scattering curve.

Moreover, it is not possible to neglect the possibility that mortalin solution structure can be represented by a combination of the *E. coli* DnaK in which the PBD is in the open (PDB

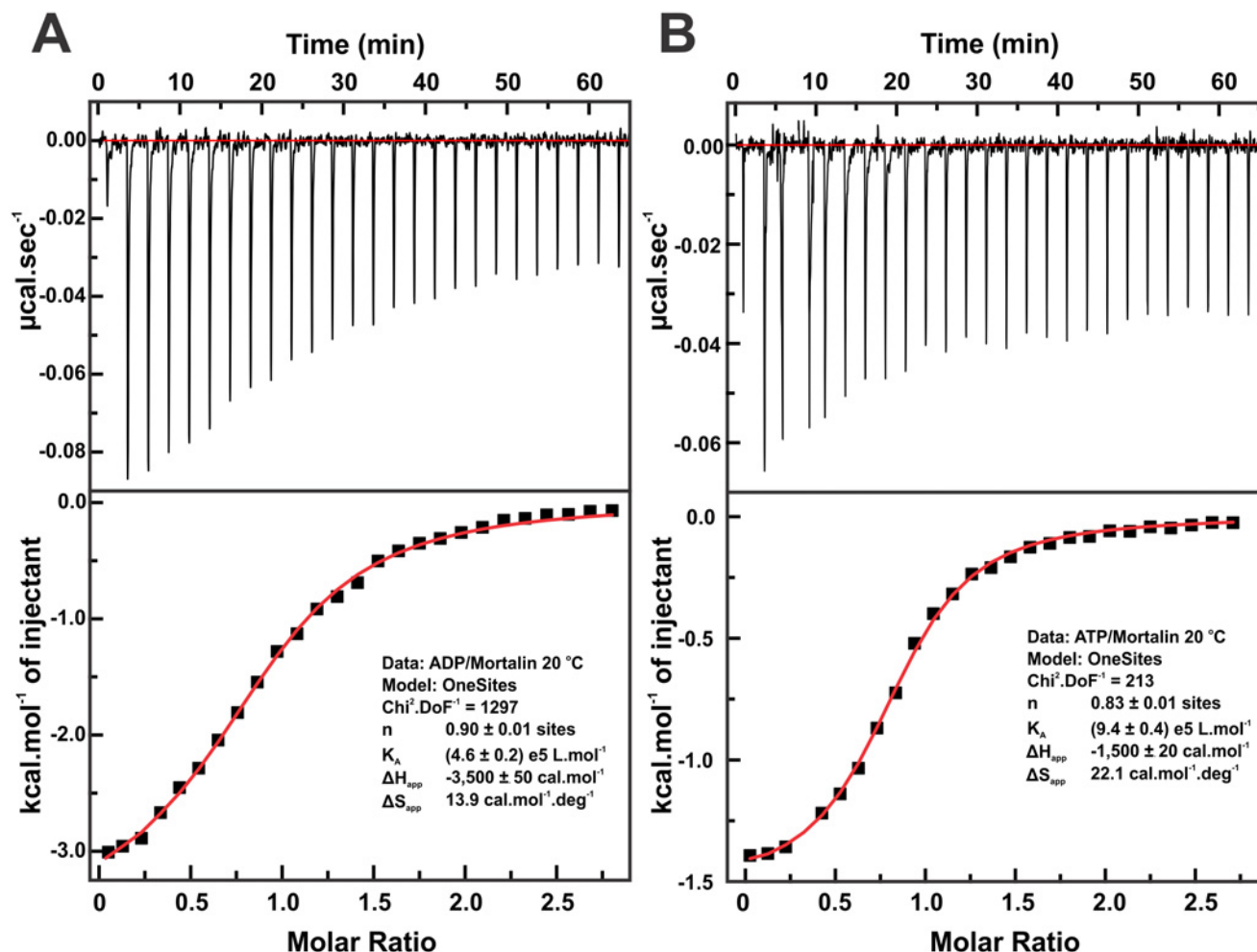


Fig 5. Mortalin interacts with ADP and ATP in a micromolar dissociation constant range. The mortalin interaction with ADP (A) and ATP (B) in the presence of Mg²⁺ was tested by ITC, suggesting K_{Ds} values of approximately 2.2 ± 0.1 µmol.L⁻¹ and 1.1 ± 0.1 µmol.L⁻¹, respectively. Moreover, the ITC data suggested that the interaction was directed by both enthalpy and entropy. *Upper panel:* The heat released at each ADP or ATP titration is presented by the negative peaks. The red line represents the baseline. *Lower panel:* The ΔH_{app} values were calculated by the integrated area of each ADP or ATP titration peak of the upper panel and plotted against the ADP/mortalin molar ratio. The red line represents the fit obtained by the one-site-binding model provided by the Origin program supplied with the ITC device in both cases. The fitting parameters are shown.

doi:10.1371/journal.pone.0117170.g005

Table 3. Summary of the T_m transitions determined to mortalin by CD_{222 nm} in the presence of adenosine nucleotides and/or Mg²⁺.

Mortalin plus ligands (200 µmol.L ⁻¹)			T _{m1} (°C)	T _{m2} (°C)
ATP	ADP	Mg ²⁺		
-	-	-	40.1 ± 0.6	73.1 ± 0.9
+	-	-	41.4 ± 0.8	72 ± 1
-	+	-	40.4 ± 0.8	71.1 ± 0.6
-	-	+	40.5 ± 0.7	73.9 ± 0.8
+	-	+	46.4 ± 0.6	71.6 ± 0.5
-	+	+	43.7 ± 0.7	70 ± 1

Values obtained by averaging 4 independent preparations.

doi:10.1371/journal.pone.0117170.t003

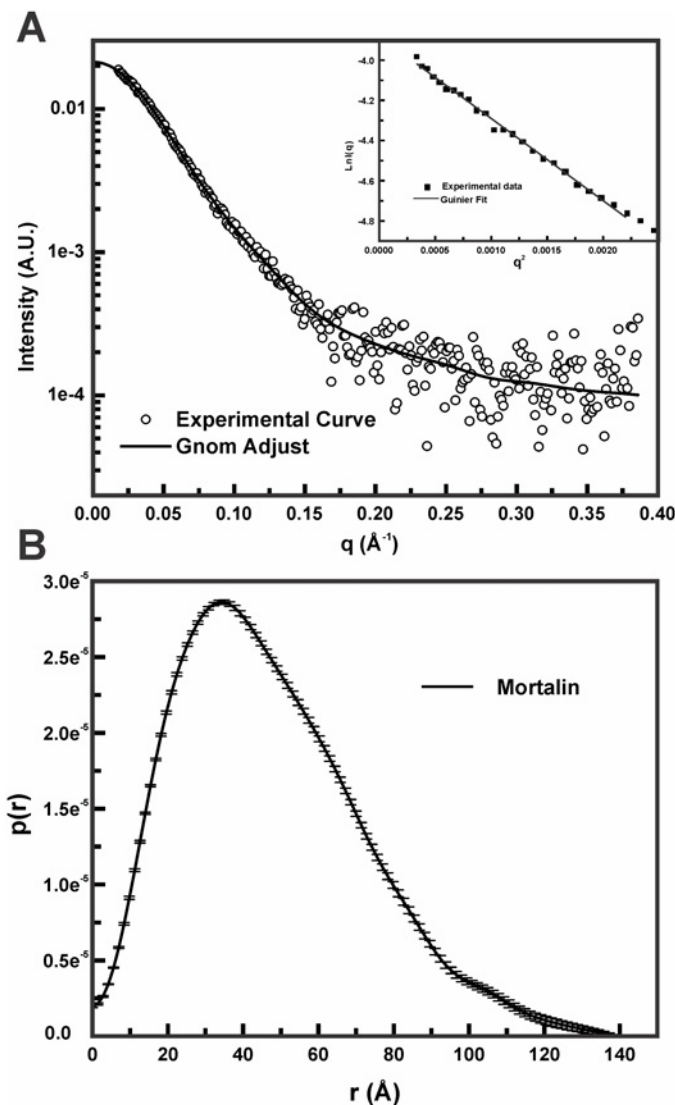


Fig 6. Mortalin has an elongated shape in solution. A) Experimental mortalin SAXS curve (open circles) suggesting that it behaved as a monodisperse system, as was confirmed by the evaluation of the Guinier region of the curve (*inset*). The GNOM fit is represented by a black line. Based on Guinier' law (red line—*inset*), mortalin had a R_g value of $36 \pm 2 \text{ \AA}$ (see text for details). **B)** The SAXS data were used to generate the $p(r)$ distribution curve, which indicated that mortalin has a prolate shape and a D_{\max} value of $130 \pm 10 \text{ \AA}$.

doi:10.1371/journal.pone.0117170.g006

acc. n. 4B9Q [46]) and in the closed (PDB acc. n. 2KHO [47]) structures. In order to check for such possibility, we used the full length DnaK structures and GENFIT software [48] to elucidate if the combinations of these structures are present in mortalin apo solutions. According to our data analysis, the mortalin SAXS curve was fitted supposing such possibility (data not shown), considering that almost 85% of the mortalin molecules were in the closed conformation, whereas 15% were in the open conformation. Therefore, in the conditions tested, mortalin behaves as equilibrium of, at least, two conformations where the PBD conformational equilibrium was dislocated to the closed conformation.

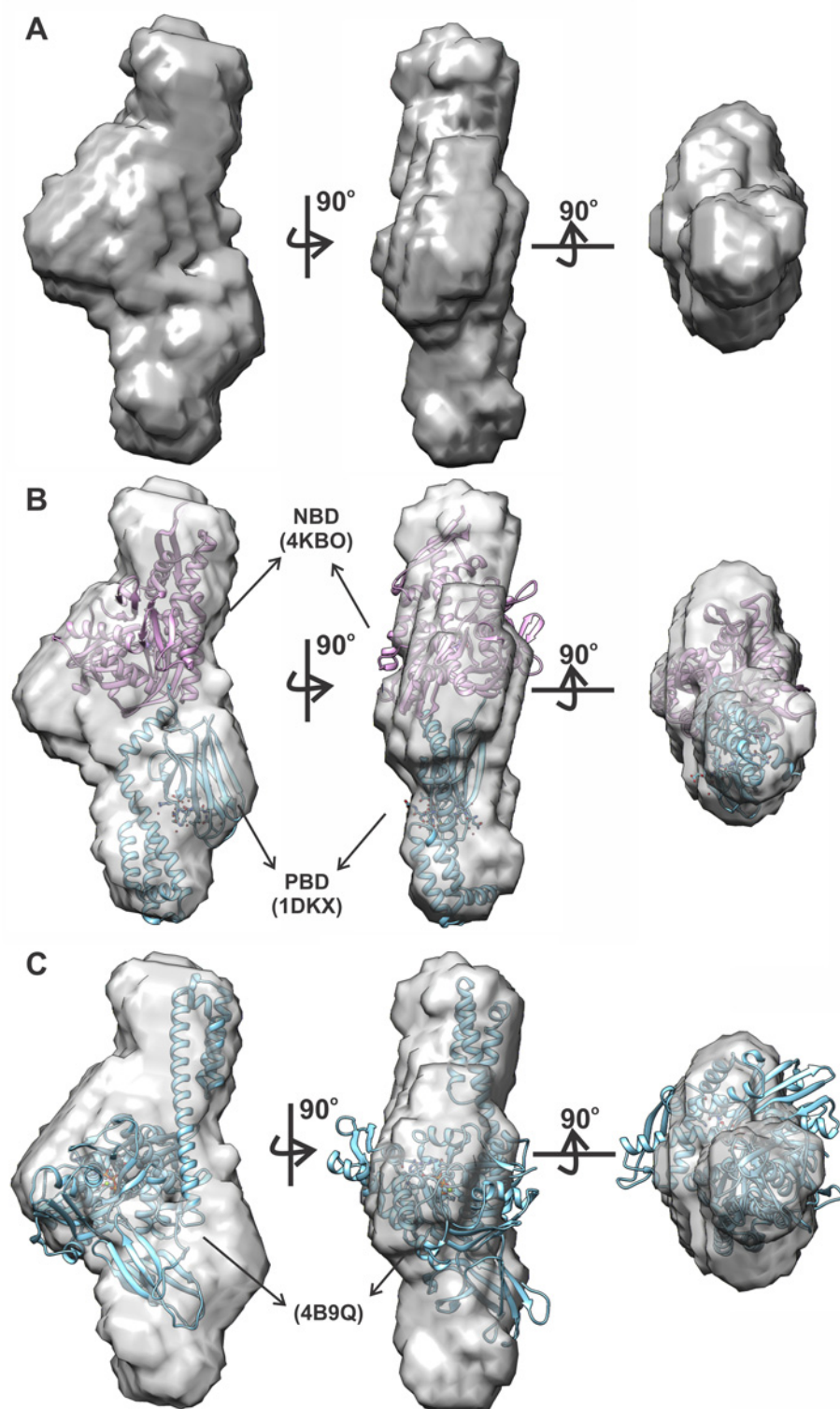


Fig 7. Mortalin *ab initio* models. The mortalin SAXS curve was used by calculating 20 low-resolution *ab initio* models using the DAMMIN software, and these were merged using the DAMAVER package. The result is the final *ab initio* model presented in several orientations (A). Manual superposition of the crystallographic structures of the mortalin NBD (PDB acc. no. 4KBO—magenta) and PBD of the *E. coli* DnaK (PDB acc. no. 1DKX—blue) into the *ab initio* model (B). Manual superposition of the crystallographic structure of the full

length *E. coli* DnaK (PDB acc. n. 4B9Q—blue) into the mortalin *ab initio* model (C). Figures generated by the UCSF Chimera software (version 1.9).

doi:10.1371/journal.pone.0117170.g007

Mortalin is formed by domains with different stabilities

Through a similarity alignment to other Hsp70s, the mortalin primary structure points to two conserved domains [22]. To study the mortalin domain organization and stability, we made use of thermal-induced unfolding strategies. We followed both the secondary and tertiary structures of mortalin by CD and intrinsic fluorescence emission, respectively. Fig. 8A shows the data for mortalin thermal-induced unfolding followed by CD_{222 nm}, which show at least two well-defined transitions. The first transition, which was represented by the loss of 20% of the CD_{222 nm} signal, had a T_{m1} centered at 40°C. This value was 5–6°C less than that reported for the T_{m1} of human cytosolic Hsp70–1A, which has three thermal transitions [37]. The second transition represented a forfeiture of approximately 30% and presented a T_{m2} of approximately 73°C. Interestingly, the CD signal was maintained at approximately -5.000 deg.cm².dmol⁻¹ at 90°C, suggesting that mortalin could retain part of its secondary structure, even at high temperatures. Human cytosolic Hsp70–1A also has a discrete thermal transition centered at 68°C and a third transition at temperatures higher than 80°C [37]. Mortalin likely presents similar thermal induced unfolding in a number of events, but we did not observe the third transition by CD_{222 nm}. Interestingly, *E. coli* DnaK thermal induced unfolding followed by CD_{222 nm} also unfolding through two transitions with similar T_ms to those observed for mortalin [59–61].

We also followed the thermal-induced unfolding of mortalin by fluorescence emission using the <λ>-signal as a probe (Fig. 8B). As expected, the temperature increment led to mortalin fluorescence emission quenching due to the water effects (Fig. 8B—inset). However, the mortalin <λ>-signal showed a blue-shift transition followed by a red-shift as a function of the temperature, whereas the <λ>-signal of the N-acetyl-tryptophanamide showed no change as a function of the temperature.

The thermal transitions observed for mortalin by fluorescence emission were centered at 43 and 77°C, respectively. Despite the T_ms being slightly higher than those observed by CD_{222 nm}, the T_ms were inside the experimental error, in agreement with the values observed by CD_{222 nm}, suggesting the correlation of these events in both the secondary and tertiary structures of mortalin. However, the Trp is located in just one of the domains (NBD), but it was apparently affected by the thermal unfolding of both domains or the unfolding of NBD in two transitions. We also performed the same experiment with Hsp70–1A and observed two red-shift transitions (Fig. 8B) with T_ms that were similar to those reported for the thermal-induced experiments followed by CD_{222 nm} [37].

The blue-shift transition observed for mortalin promptly suggests that thermal-induced unfolding led to mortalin NBD packing and/or association/aggregation. This event may be mediated by the NBD because the single mortalin Trp is located in this domain. Therefore, the apo NBD of mortalin, under the conditions tested here, appears to be prone to aggregate at temperatures close to the physiological temperatures or in fever states. Interestingly, it has been reported that Hsp70 aggregates when it is thermally unfolded [52]. Specifically, it has been shown that mortalin has an aggregation tendency that is dependent on its NBD [32]. Taken altogether, these results indicate that mortalin has different domain stabilities and could unfold by a slightly different mechanism in comparison to Hsp70–1A.

The effect of adenosine nucleotides (200 μmol.L⁻¹) and/or Mg²⁺ (200 μmol.L⁻¹) on mortalin stability was investigated using thermal-induced unfolding followed by CD_{222 nm}. The thermal-unfolding profiles in the presence of these ligands were similar (data not shown) to those

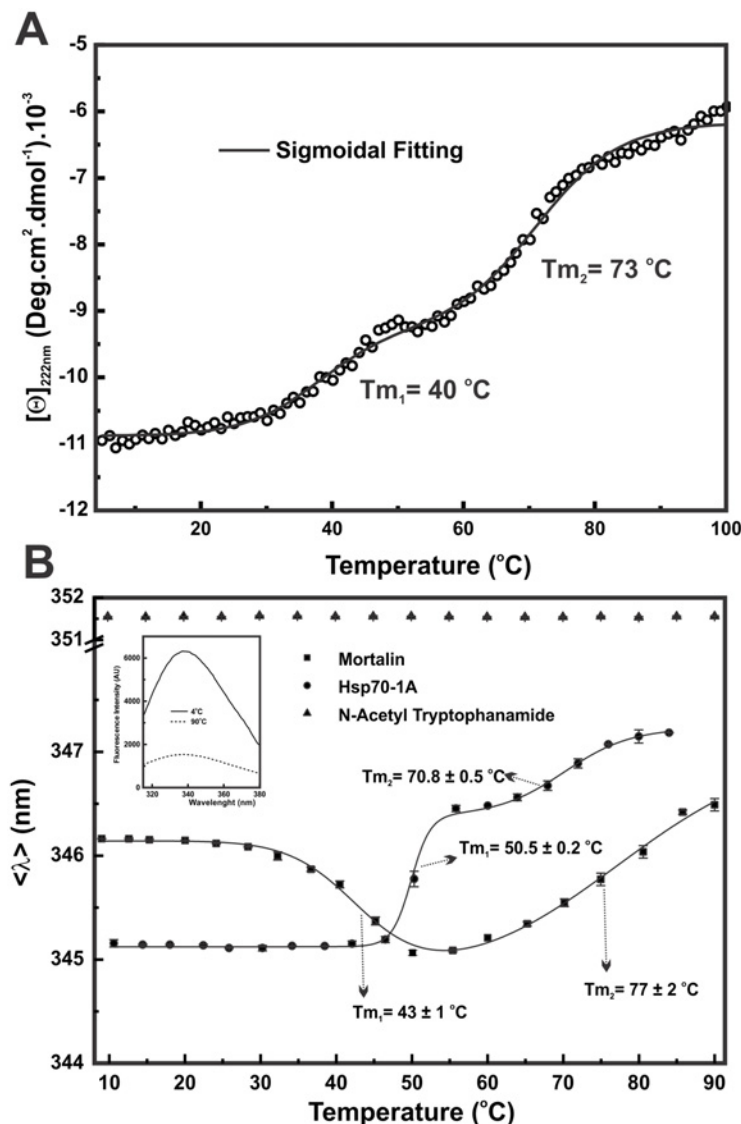


Fig 8. Mortalin is composed of at least two domains with different stabilities. **A)** The thermal-induced unfolding of mortalin followed by CD_{222 nm} presented two well-defined transitions with T_m values centered at 40 and 73°C; however, mortalin did not unfold completely (see text for details). **B)** Thermal-induced unfolding of mortalin followed by intrinsic fluorescence emission and represented as the $\langle \lambda \rangle$ -signal showing that mortalin suffered two blue-shift transitions with T_m values of approximately 43 and 77°C. Hsp70–1A presented two red-shift transitions with T_m values at 50.5 and 70.8°C. N-acetyl tryptophanamide at the same buffer conditions was used, as a control, and no transitions were observed at the $\langle \lambda \rangle$ -signal (351.5 ± 0.2 nm). The blue-shift transition suggested that mortalin associated or aggregated in the thermal-induced unfolding experiments (see text for details).

doi:10.1371/journal.pone.0117170.g008

found in the absence of these ligands (Fig. 8A), and Table 3 summarizes the T_ms estimated in the absence and presence of different combinations of ligands. Surprisingly, the presence of Mg²⁺, ADP or ATP alone did not induce significant changes in either T_{m1} or T_{m2} (Table 3). These results contrast those observed for human cytosolic Hsp70–1A [37], where the adenosine nucleotides alone increased the first thermal-induced transition by approximately 4°C followed by CD_{222 nm} under similar conditions. Nonetheless, the combination of ATP-Mg²⁺ or ADP-Mg²⁺ increased the T_{m1} of mortalin to 46°C and 44°C, respectively, resulting in an

increment of 4–6°C in the T_{m1} (Table 3). For human Hsp70–1A, the combination of adenosine nucleotides and Mg^{2+} ions also led to an additional increment in the first T_m of 7–9°C [37], indicating the importance of the Mg^{2+} ions for adenosine nucleotide binding. These results suggested that adenosine nucleotides bind to mortalin and stabilize the NBD structure.

Discussion

In this manuscript, we report the production and purification of recombinant human mortalin in its monomeric and functional form without the use of unfolding/refolding strategies. Recombinant mortalin production was reached by its co-expression with the hHep1 co-chaperone, which maintains mortalin in the supernatant of the lysed *E. coli* cells [34]. For purification purposes, the mortalin was cloned into a pET28a expression vector, and hHep1 was cloned into a pET23a expression vector, which produces hHep1 in undetectable amounts (data not shown), as was reported by a previous study [32]. This allowed the production of mortalin samples with substoichiometric and/or undetectable amounts of hHep1, as attested by the SDS-PAGE figures and the MM determinations by aSEC, AUC and SAXS techniques.

To attest that mortalin was produced and purified in its functional state, enzyme kinetics experiments were performed to evaluate the basal ATPase activity of mortalin compared with that of Hsp70–1A. We observed that mortalin had a slightly higher ATPase activity than Hsp70–1A, but both proteins presented them in the same order of magnitude than other Hsp70s. We also observed that both proteins had K_M values in the higher $\mu\text{mol.L}^{-1}$ range. We also tested if the ATPase activity of mortalin and Hsp70–1A was stimulated by the NR peptide. The results pointed out that mortalin and Hsp70–1A presented, at NR peptide saturation, increments of 25% and 15% on their basal ATPase activity, respectively, indicating that both recombinant proteins were produced in their allosterically forms. Nevertheless, they have showed some differences in client protein specificities since the EC_{50} registered for mortalin was approximately 25 times lower than for Hsp70–1A. The NR peptide has been used as client protein model for *E. coli* DnaK [58] and similar ATPase stimulation was also reached for this protein at 100 $\mu\text{mol.L}^{-1}$ NR peptide [62]. These results also indicate that human recombinant mortalin is functionally similar to *E. coli* DnaK (see below).

ITC experiments were performed to test the interaction of mortalin with adenosine nucleotides. Because mortalin has weak ATPase activity, we used ATP in these experiments instead of a non-hydrolysable ATP analogue. The results indicated that mortalin interacts with ATP and ADP at a low micromolar K_D range and that the interaction is driven by enthalpy and entropy, as was also observed for human cytosolic Hsp70–1A [37]. In contrast to the latter, the interaction of mortalin with adenosine nucleotides was dependent on the presence of Mg^{2+} ions, as indicated by the thermal-induced unfolding experiments and the T_m s (Table 3). Moreover, only two well-defined thermal transitions were observed for mortalin, whereas three transitions were reported for Hsp70–1A [37]. Therefore, these two proteins present different stabilities.

We characterized the recombinant mortalin by several biophysical tools and observed properties that are similar to those reported for other Hsp70 proteins [37]. It is constituted by α -helix and β -sheet secondary structures, as estimated by circular dichroism experiments. The single Trp residue located in the NBD is at least partially protected from the solvent, suggesting that this residue is buried in the protein hydrophobic interior. Our production strategy also allowed us to obtain mortalin in its monomeric form at least 24 h after purification by preparative SEC and at low protein concentrations. We observed that both storage at 4°C and high concentration induced mortalin to undergo self-association and/or aggregation processes (data not shown), which limits its study. Furthermore, the mortalin monomeric form has a slightly elongated shape, as attested by the aSEC, AUC and SAXS results. Human cytosolic Hsp70–1A was also

studied by AUC and had a $s_{20,w}^0$ of approximately 4.4 S in the nucleotide-free state [51]. This value was slightly lower than the value observed for mortalin despite the similar MM and experimental conditions, which indicated that mortalin is slightly more globular than Hsp70-1A.

We also obtained SAXS data for mortalin in the monomeric state, which allowed the generation of a low-resolution model. The structural and hydrodynamic properties of this model were in accordance with the hydrodynamic and structural properties determined experimentally, indicating that the low-resolution model for mortalin was reliable. It is worth noting that the *ab initio* model suggests that the mortalin domains should be coupled to each other even in the absence of nucleotides because the central part of the model is enlarged in relation to the ends. Besides, the low resolution model obtained for mortalin from SAXS curve in apo conditions adequately accommodated the crystallographic structures of mortalin NBD and *E. coli* PBD, which resembles the ADP bound state (Fig. 7B). However, the mortalin *ab initio* model did not properly adjust the X-ray structure of *E. coli* DnaK bound to ATP, in which the PBD is in the open conformation. Actually, the mortalin SAXS curve was fitted regarding that it represents a conformational equilibrium between, at least two conformations, in which the PBD is in the open and closed conformations.

We employed unfolding strategies to monitor the domain organization of mortalin. Thermal-induced unfolding followed by CD_{222 nm} indicated that mortalin is composed of at least two domains because two well-determined transitions were observed. Interestingly, the first transition started at 35°C and had a T_{m1} centered at 40°C in the nucleotide-free state. Thermal-induced unfolding followed by fluorescence noted a blue-shift transition at approximately the same temperature observed for CD_{222 nm}. Altogether, these results suggested that mortalin can associate during its thermal-induced unfolding. Because the NBD is related to this thermal-induced unfolding transition, its participation in mortalin self-aggregation can be hypothesized. Previous studies indicated that the first transition of Hsp70 thermal-induced unfolding involves the partial unfolding of the NBD because the presence of adenosine nucleotides increased the first T_m [37, 52, 53], as attested in this study for mortalin. Zhai et al. [32] also reported that mortalin self-aggregation depends on the NBD. Interestingly, *E. coli* DnaK also shows two transitions in the thermal-induced unfolding experiments [59–61] with comparable T_{ms} to those observed for mortalin, indicating that both proteins have domains with similar thermal stabilities. Actually, mortalin shares more identity with *E. coli* DnaK (59%) than with Hsp70-1A (48%), which can explain their similarities in thermal stabilities as well as the ATPase activity stimulation observed upon NR peptide titration.

Altogether, despite the challenges associated with the production of mortalin in its monomeric form and functional state, this work shed light on the mortalin structure and dynamics and indicates a strategy for the production of functional mortalin in sufficient amounts to perform additional functional studies. An allosteric pocket of Hsp70 proteins was recently identified as a promising site for structure-based drug design [63], and our study may help one to identify whether this binding site is also present in human mortalin and to test the interaction of mortalin with its specific inhibitor [29, 64]. Interaction studies of mortalin with inhibitor compounds and certain of its mitochondrial co-chaperones are underway.

Acknowledgments

We acknowledge the Spectroscopy and Calorimetry Laboratory at Brazilian Biosciences National Laboratory (LNBio/CNPq-ABTLuS, Campinas, Brazil) for making available the AUC device. CHIR and LRSB thank FAPESP and CNPq for financial support. We also thank the Brazilian Synchrotron Light Laboratory (LNLS/CNPq-ABTLuS, Campinas, Brazil) for the use of the SAXS beamline.

Author Contributions

Conceived and designed the experiments: JCB CHIR PRDS. Performed the experiments: JCB PRDS. Analyzed the data: JCB PRDS LRSB. Contributed reagents/materials/analysis tools: JCB CHIR. Wrote the paper: JCB PRDS CHIR.

References

1. Wadhwa R, Kaul SC, Ikawa Y, Sugimoto Y (1993) Identification of a novel member of mouse hsp70 family. Its association with cellular mortal phenotype. *J Biol Chem* 268: 6615–6621. PMID: [8454632](#)
2. Bhattacharyya T, Karnezis AN, Murphy SP, Hoang T, Freeman BC, et al. (1995) Cloning and Subcellular Localization of Human Mitochondrial hsp70. *J Biol Chem* 270: 1705–1710. doi: [10.1074/jbc.270.4.1705](#) PMID: [7829505](#)
3. Domanico SZ, DeNagel DC, Dahlseid JN, Green JM, Pierce SK (1993) Cloning of the gene encoding peptide-binding protein 74 shows that it is a new member of the heat shock protein 70 family. *Mol Cell Biol* 13: 3598–3610. PMID: [7684501](#)
4. Londono C, Osorio C, Gama V, Alzate O (2012) Mortalin, Apoptosis, and Neurodegeneration. *Biomolecules* 2: 143–164. doi: [10.3390/biom2010143](#) PMID: [24970131](#)
5. Wadhwa R, Sugihara T, Yoshida A, Nomura H, Reddel RR, et al. (2000) Selective toxicity of MKT-077 to cancer cells is mediated by its binding to the hsp70 family protein mot-2 and reactivation of p53 function. *Cancer Res* 60: 6818–6821. PMID: [11156371](#)
6. Wadhwa R, Yaguchi T, Hasan K, Mitsui Y, Reddel RR, et al. (2002) Hsp70 family member, mot-2/mthsp70/GRP75, binds to the cytoplasmic sequestration domain of the p53 protein. *Exp Cell Res* 274: 246–253. doi: [10.1006/excr.2002.5468](#) PMID: [11900485](#)
7. Kaul SC, Deocaris CC, Wadhwa R (2007) Three faces of mortalin: A housekeeper, guardian and killer. *Exp Gerontol* 42: 263–274. doi: [10.1016/j.exger.2006.10.020](#) PMID: [17188442](#)
8. Fan ACY, Young JC (2011) Function of Cytosolic Chaperones in Tom70-Mediated Mitochondrial Import. *Prot Pept Lett* 18: 122–131. doi: [10.2174/092986611794475020](#)
9. Dolezal P, Likic V, Tachezy J, Lithgow T (2006) Evolution of the molecular machines for protein import into mitochondria. *Science* 313: 314–318. doi: [10.1126/science.1127895](#) PMID: [16857931](#)
10. Mokranjac D, Neupert W (2009) Thirty years of protein translocation into mitochondria: Unexpectedly complex and still puzzling. *BBA-Mol Cell Res* 1793: 33–41.
11. Bohnert M, Pfanner N, van der Laan M (2007) A dynamic machinery for import of mitochondrial precursor proteins. *Febs Lett* 581: 2802–2810. doi: [10.1016/j.febslet.2007.03.004](#) PMID: [17376437](#)
12. Kaul SC, Reddel RR, Sugihara T, Mitsui Y, Wadhwa R (2000) Inactivation of p53 and life span extension of human diploid fibroblasts by mot-2. *Febs Lett* 474: 159–164. doi: [10.1016/S0014-5793\(00\)01594-5](#)
13. Wadhwa R, Takano S, Kaur K, Deocaris CC, Pereira-Smith OM, et al. (2006) Upregulation of mortalin/mthsp70/Grp75 contributes to human carcinogenesis. *Inter J Cancer* 118: 2973–2980. doi: [10.1002/ijc.21773](#)
14. Qu M, Zhou Z, Xu S, Chen C, Yu Z, et al. (2011) Mortalin overexpression attenuates beta-amyloid-induced neurotoxicity in SH-SY5Y cells. *Brain Res* 1368: 336–345. doi: [10.1016/j.brainres.2010.10.068](#) PMID: [20974113](#)
15. Liu Y, Liu W, Song XD, Zuo J (2005) Effect of GRP75/mthsp70/PBP74/mortalin overexpression on intracellular ATP level, mitochondrial membrane potential and ROS accumulation following glucose deprivation in PC12 cells. *Mol Cell Biochem* 268: 45–51. doi: [10.1007/s11010-005-2996-1](#) PMID: [15724436](#)
16. Jin JH, Hulette C, Wang Y, Zhang T, Pan C, et al. (2006) Proteomic identification of a stress protein, mortalin/mthsp70/GRP75—Relevance to Parkinson disease. *Mol Cell Proteomics* 5: 1193–1204. doi: [10.1074/mcp.M500382-MCP200](#) PMID: [16565515](#)
17. Xu L, Voloboueva LA, Ouyang Y, Emery JF, Giffard RG (2008) Overexpression of mitochondrial Hsp70/Hsp75 in rat brain protects mitochondria, reduces oxidative stress, and protects from focal ischemia. *J Cereb Blood Flow Metab* 29: 365–374. doi: [10.1038/jcbfm.2008.125](#) PMID: [18985056](#)
18. Wadhwa R, Takano S, Kaur K, Aida S, Yaguchi T, et al. (2005) Identification and characterization of molecular interactions between mortalin/mtHsp70 and HSP60. *Biochem J* 391: 185–190. doi: [10.1042/BJ20050861](#) PMID: [15957980](#)
19. Rehling P, Brandner K, Pfanner N (2004) Mitochondrial import and the twin-pore translocase. *Nat Rev Mol Cell Biol* 5: 519–530. doi: [10.1038/nrm1426](#) PMID: [15232570](#)

20. Wegele H, Muller L, Buchner J (2004) Hsp70 and Hsp90—a relay team for protein folding. *Rev Physiol Biochem Pharmacol* 151: 1–44. doi: [10.1007/s10254-003-0021-1](https://doi.org/10.1007/s10254-003-0021-1) PMID: [14740253](https://pubmed.ncbi.nlm.nih.gov/14740253/)
21. Soti C, Nagy E, Giricz Z, Vigh L, Csermely P, et al. (2005) Heat shock proteins as emerging therapeutic targets. *Br J Pharmacol* 146: 769–780. doi: [10.1038/sj.bjp.0706396](https://doi.org/10.1038/sj.bjp.0706396) PMID: [16170327](https://pubmed.ncbi.nlm.nih.gov/16170327/)
22. da Silva KP, Borges JC (2011) The Molecular Chaperone Hsp70 Family Members Function by a Bidirectional Heterotrophic Allosteric Mechanism. *Protein Pept Lett* 18: 132–142. doi: [10.2174/092986611794475057](https://doi.org/10.2174/092986611794475057) PMID: [21121894](https://pubmed.ncbi.nlm.nih.gov/21121894/)
23. Broadley SA, Hartl FU (2009) The role of molecular chaperones in human misfolding diseases. *FEBS Lett* 583: 2647–2653. doi: [10.1016/j.febslet.2009.04.029](https://doi.org/10.1016/j.febslet.2009.04.029) PMID: [19393652](https://pubmed.ncbi.nlm.nih.gov/19393652/)
24. Deocaris CC, Kaul SC, Wadhwa R (2012) Mortalin's Machinery. In: Sunil C. Kaul, Renu Wadhwa, editors. *Mortalin Biology: Life, Stress and Death*. Springer. pp. 21–30.
25. Wadhwa R, Kaul SC, Sugimoto Y, Mitsui Y (1993) Induction of Cellular Senescence by Transfection of Cytosolic Mortalin Cdn in Nih-3T3-Cells. *J Biol Chem* 268: 22239–22242. PMID: [7693662](https://pubmed.ncbi.nlm.nih.gov/7693662/)
26. Deocaris CC, Kaul SC, Wadhwa R (2012) Mortalin's Machinery. In: Kaul SC, Wadhwa R, editors. *Mortalin biology: life, stress and death*. New York: Dordrecht: Springer, c2012. pp. 21–30.
27. Wadhwa R, Kaul SC, Mitsui Y, Sugimoto Y (1993) Differential Subcellular-Distribution of Mortalin in Mortal and Immortal Mouse and Human Fibroblasts. *Exp Cell Res* 207: 442–448. doi: [10.1006/excr.1993.1213](https://doi.org/10.1006/excr.1993.1213) PMID: [8344392](https://pubmed.ncbi.nlm.nih.gov/8344392/)
28. Ran QT, Wadhwa R, Kawai R, Kaul SC, Sifers RN, et al. (2000) Extramitochondrial localization of mortalin/mthsp70/PBP74/GRP75. *Biochem Biophys Res Comm* 275: 174–179. doi: [10.1006/bbrc.2000.3237](https://doi.org/10.1006/bbrc.2000.3237) PMID: [10944461](https://pubmed.ncbi.nlm.nih.gov/10944461/)
29. Deocaris CC, Widodo N, Shrestha BG, Kaur K, Ohtaka M, et al. (2007) Mortalin sensitizes human cancer cells to MKT-077-induced senescence. *Cancer Lett* 252: 259–269. doi: [10.1016/j.canlet.2006.12.038](https://doi.org/10.1016/j.canlet.2006.12.038) PMID: [17306926](https://pubmed.ncbi.nlm.nih.gov/17306926/)
30. Szklarz LKS, Guiard B, Rissler M, Wiedemann N, Kozjak V, et al. (2005) Inactivation of the mitochondrial heat shock protein Zim17 leads to aggregation of matrix Hsp70s followed by pleiotropic effects on morphology and protein biogenesis. *J Mol Biol* 351: 206–218. doi: [10.1016/j.jmb.2005.05.068](https://doi.org/10.1016/j.jmb.2005.05.068)
31. Sichting M, Mokranjac D, Azem A, Neupert W, Hell K (2005) Maintenance of structure and function of mitochondrial Hsp70 chaperones requires the chaperone Hep1. *EMBO J* 24: 1046–1056. doi: [10.1038/sj.emboj.7600580](https://doi.org/10.1038/sj.emboj.7600580) PMID: [15719019](https://pubmed.ncbi.nlm.nih.gov/15719019/)
32. Zhai P, Stanworth C, Liu S, Silberg JJ (2008) The human escort protein hep binds to the ATPase domain of mitochondrial Hsp70 and regulates ATP hydrolysis. *J Biol Chem* 283: 26098–26106. doi: [10.1074/jbc.M803475200](https://doi.org/10.1074/jbc.M803475200) PMID: [18632665](https://pubmed.ncbi.nlm.nih.gov/18632665/)
33. Luo WI, Dizin E, Yoon T, Cowan JA (2010) Kinetic and structural characterization of human mortalin. *Protein Expr Purif* 72: 75–81. doi: [10.1016/j.pep.2010.02.003](https://doi.org/10.1016/j.pep.2010.02.003) PMID: [20152901](https://pubmed.ncbi.nlm.nih.gov/20152901/)
34. Dores-Silva PR, Minari K, Ramos CHI, Barbosa LRS, Borges JC (2013) Structural and stability studies of the human mtHsp70-escort protein 1: An essential mortalin co-chaperone. *Int J Biol Macromol* 56: 140–148. doi: [10.1016/j.ijbiomac.2013.02.009](https://doi.org/10.1016/j.ijbiomac.2013.02.009) PMID: [23462535](https://pubmed.ncbi.nlm.nih.gov/23462535/)
35. Vu MT, Zhai P, Lee J, Guerra C, Liu S, et al. (2012) The DNLZ/HEP zinc-binding subdomain is critical for regulation of the mitochondrial chaperone HSPA9. *Protein Sci* 21: 258–267. doi: [10.1002/pro.2012](https://doi.org/10.1002/pro.2012) PMID: [22162012](https://pubmed.ncbi.nlm.nih.gov/22162012/)
36. Zhai P, Vu MT, Hoff KG, Silberg JJ (2011) A conserved histidine in human DNLZ/HEP is required for stimulation of HSPA9 ATPase activity. *Biochem Biophys Res Comm* 408: 589–594. doi: [10.1016/j.bbrc.2011.04.066](https://doi.org/10.1016/j.bbrc.2011.04.066)
37. Borges JC, Ramos CHI (2006) Spectroscopic and thermodynamic measurements of nucleotide-induced changes in the human 70-kDa heat shock cognate protein. *Arch Biochem Biophys* 452: 46–54. doi: [10.1016/j.abb.2006.05.006](https://doi.org/10.1016/j.abb.2006.05.006) PMID: [16806043](https://pubmed.ncbi.nlm.nih.gov/16806043/)
38. Bohm G, Muhr R, Jaenicke R (1992) Quantitative-Analysis of Protein Far Uv Circular-Dichroism Spectra by Neural Networks. *Protein Eng* 5: 191–195. doi: [10.1093/protein/5.3.191](https://doi.org/10.1093/protein/5.3.191) PMID: [1409538](https://pubmed.ncbi.nlm.nih.gov/1409538/)
39. Lebowitz J, Lewis MS, Schuck P (2002) Modern analytical ultracentrifugation in protein science: A tutorial review. *Protein Sci* 11: 2067–2079. doi: [10.1110/ps.0207702](https://doi.org/10.1110/ps.0207702) PMID: [12192063](https://pubmed.ncbi.nlm.nih.gov/12192063/)
40. Schuck P, Perugini MA, Gonzales NR, Howlett GJ, Schubert D (2002) Size-distribution analysis of proteins by analytical ultracentrifugation: Strategies and application to model systems. *Biophys J* 82: 1096–1111. doi: [10.1016/S0006-3495\(02\)75469-6](https://doi.org/10.1016/S0006-3495(02)75469-6) PMID: [11806949](https://pubmed.ncbi.nlm.nih.gov/11806949/)
41. Borges JC, Ramos CHI (2011) Analysis of molecular targets of mycobacterium tuberculosis by analytical ultracentrifugation. *Curr Med Chem* 18: 1276–1285. doi: [10.2174/092986711795029537](https://doi.org/10.2174/092986711795029537) PMID: [21366535](https://pubmed.ncbi.nlm.nih.gov/21366535/)

42. Orthaber D, Bergmann A, Glatter O (2000) SAXS experiments on absolute scale with Kratky systems using water as a secondary standard. *J Appl Cryst* 33: 218–225. doi: [10.1107/S0021889899015216](https://doi.org/10.1107/S0021889899015216)
43. Svergun DI (1999) Restoring low resolution structure of biological macromolecules from solution scattering using simulated annealing. *Biophys J* 76: 2879–2886. doi: [10.1016/S0006-3495\(99\)77443-6](https://doi.org/10.1016/S0006-3495(99)77443-6) PMID: [10354416](https://pubmed.ncbi.nlm.nih.gov/10354416/)
44. Volkov VV, Svergun DI (2003) Uniqueness of ab initio shape determination in small-angle scattering. *J Appl Cryst* 36: 860–864. doi: [10.1107/S0021889803000268](https://doi.org/10.1107/S0021889803000268)
45. de la Torre JG, Huertas ML, Carrasco B (2000) Calculation of hydrodynamic properties of globular proteins from their atomic-level structure. *Biophys J* 78: 719–730. doi: [10.1016/S0006-3495\(00\)76630-6](https://doi.org/10.1016/S0006-3495(00)76630-6)
46. Kityk R, Kopp J, Sinning I, Mayer MP (2012) Structure and Dynamics of the ATP-Bound Open Conformation of Hsp70 Chaperones. *Mol Cell* 48: 863–874. doi: [10.1016/j.molcel.2012.09.023](https://doi.org/10.1016/j.molcel.2012.09.023) PMID: [23123194](https://pubmed.ncbi.nlm.nih.gov/23123194/)
47. Bertelsen EB, Chang L, Gestwicki JE, Zuiderweg ERP (2009) Solution conformation of wild-type E. coli Hsp70 (DnaK) chaperone complexed with ADP and substrate. *Proc Natl Acad Sci U S A* 106: 8471–8476. doi: [10.1073/pnas.0903503106](https://doi.org/10.1073/pnas.0903503106) PMID: [19439666](https://pubmed.ncbi.nlm.nih.gov/19439666/)
48. Spinozzi F, Ferrero C, Ortore MG, De Maria Antolinos A, Mariani P (2014) GENFIT: software for the analysis of small-angle X-ray and neutron scattering data of macromolecules in solution. *J Appl Cryst* 47: 1132–1139. doi: [10.1107/S1600576714005147](https://doi.org/10.1107/S1600576714005147)
49. Ortore MG, Spinozzi F, Mariani P, Paciaroni A, Barbosa LRS, et al. (2009) Combining structure and dynamics: non-denaturing high-pressure effect on lysozyme in solution. *J R Soc Interface* 6: S619–S634. doi: [10.1098/rsif.2009.0163.focus](https://doi.org/10.1098/rsif.2009.0163.focus) PMID: [19570795](https://pubmed.ncbi.nlm.nih.gov/19570795/)
50. Silva KP, Seraphim TV, Borges JC (2013) Structural and functional studies of *Leishmania braziliensis* Hsp90. *BBA—Proteins Proteom* 1834: 351–361. doi: [10.1016/j.bbapap.2012.08.004](https://doi.org/10.1016/j.bbapap.2012.08.004)
51. Borges JC, Ramos CHI (2009) Characterization of nucleotide-induced changes on the quaternary structure of human 70 kDa heat shock protein Hsp70.1 by analytical ultracentrifugation. *BMB Rep* 42: 166–171. doi: [10.5483/BMBRep.2009.42.3.166](https://doi.org/10.5483/BMBRep.2009.42.3.166) PMID: [19336004](https://pubmed.ncbi.nlm.nih.gov/19336004/)
52. Palleros DR, Welch WJ, Fink AL (1991) Interaction of hsp70 with unfolded proteins: effects of temperature and nucleotides on the kinetics of binding. *Proc Natl Acad Sci U S A* 88: 5719–5723. doi: [10.1073/pnas.88.13.5719](https://doi.org/10.1073/pnas.88.13.5719) PMID: [1829527](https://pubmed.ncbi.nlm.nih.gov/1829527/)
53. Montgomery DL, Morimoto RI, Gierasch LM (1999) Mutations in the substrate binding domain of the Escherichia coli 70 kDa molecular chaperone, DnaK, which alter substrate affinity or interdomain coupling. *J Mol Biol* 286: 915–932. doi: [10.1006/jmbi.1998.2514](https://doi.org/10.1006/jmbi.1998.2514) PMID: [10024459](https://pubmed.ncbi.nlm.nih.gov/10024459/)
54. Palleros DR, Reid KL, Shi L, Fink AL (1993) DnaK ATPase activity revisited. *Febs Letters* 336: 124–128. doi: [10.1016/0014-5793\(93\)81624-9](https://doi.org/10.1016/0014-5793(93)81624-9) PMID: [8262193](https://pubmed.ncbi.nlm.nih.gov/8262193/)
55. Kozin MB, Svergun DI (2001) Automated matching of high- and low-resolution structural models. *J Appl Cryst* 34: 33–41. doi: [10.1107/S0021889800014126](https://doi.org/10.1107/S0021889800014126)
56. Barbosa LRS, Spinozzi F, Mariani P, Itri R (2013) Small-Angle X-Ray Scattering Applied to Proteins in Solution. In: *Proteins in Solution and at Interfaces*. John Wiley & Sons, Inc. pp. 49–72.
57. Amick J, Schlanger SE, Wachnowsky C, Moseng MA, Emerson CC, et al. (2014) Crystal structure of the nucleotide-binding domain of mortalin, the mitochondrial Hsp70 chaperone. *Protein Sci* 23: 833–842. doi: [10.1002/pro.2466](https://doi.org/10.1002/pro.2466) PMID: [24687350](https://pubmed.ncbi.nlm.nih.gov/24687350/)
58. Zhu XT, Zhao X, Burkholder WF, Gragerov A, Ogata CM, et al. (1996) Structural analysis of substrate binding by the molecular chaperone DnaK. *Science* 272: 1606–1614. doi: [10.1126/science.272.5268.1606](https://doi.org/10.1126/science.272.5268.1606) PMID: [8658133](https://pubmed.ncbi.nlm.nih.gov/8658133/)
59. Vogel M, Mayer MP, Bukau B (2006) Allosteric regulation of Hsp70 chaperones involves a conserved interdomain linker. *J Biol Chem* 281: 38705–38711. doi: [10.1074/jbc.M609020200](https://doi.org/10.1074/jbc.M609020200) PMID: [17052976](https://pubmed.ncbi.nlm.nih.gov/17052976/)
60. Palleros DR, Reid KL, McCarty JS, Walker GC, Fink AL (1992) DnaK, hsp73, and their molten globules. Two different ways heat shock proteins respond to heat. *J Biol Chem* 267: 5279–5285.
61. Popp SL, Reinstein J (2009) Functional characterization of the DnaK chaperone system from the archaeon *Methanothermobacter thermautotrophicus* +öH. *FEBS Lett* 583: 573–578. doi: [10.1016/j.febslet.2008.12.062](https://doi.org/10.1016/j.febslet.2008.12.062) PMID: [19162025](https://pubmed.ncbi.nlm.nih.gov/19162025/)
62. Pellicchia M, Montgomery DL, Stevens SY, Vander Kooi CW, Feng HP, et al. (2000) Structural insights into substrate binding by the molecular chaperone DnaK. *Nat Struct Biol* 7: 298–303. doi: [10.1038/74062](https://doi.org/10.1038/74062) PMID: [10742174](https://pubmed.ncbi.nlm.nih.gov/10742174/)
63. Rodina A, Patel P, Kang Y, Patel Y, Baaklini I, et al. (2013) Identification of an Allosteric Pocket on Human Hsp70 Reveals a Mode of Inhibition of This Therapeutically Important Protein. *Chem Biol* 20: 1–12. doi: [10.1016/j.chembiol.2013.10.008](https://doi.org/10.1016/j.chembiol.2013.10.008)

64. Rousaki A, Miyata Y, Jinwal UK, Dickey CA, Gestwicki JE, et al. (2011) Allosteric Drugs: The Interaction of Antitumor Compound MKT-077 with Human Hsp70 Chaperones. *J Mol Biol* 411: 614–632. doi: [10.1016/j.jmb.2011.06.003](https://doi.org/10.1016/j.jmb.2011.06.003) PMID: [21708173](https://pubmed.ncbi.nlm.nih.gov/21708173/)
65. McCarty JS, Walker GC (1991) DnaK as a thermometer: threonine-199 is site of autophosphorylation and is critical for ATPase activity. *Proc Natl Acad Sci U S A* 88: 9513–9517. doi: [10.1073/pnas.88.21.9513](https://doi.org/10.1073/pnas.88.21.9513) PMID: [1835085](https://pubmed.ncbi.nlm.nih.gov/1835085/)
66. Silberg JJ, Vickery LE (2000) Kinetic Characterization of the ATPase Cycle of the Molecular Chaperone Hsc66 from *Escherichia coli*. *J Biol Chem* 275: 7779–7786. doi: [10.1074/jbc.275.11.7779](https://doi.org/10.1074/jbc.275.11.7779) PMID: [10713091](https://pubmed.ncbi.nlm.nih.gov/10713091/)
67. Sadis S, Hightower LE (1992) Unfolded proteins stimulate molecular chaperone Hsc70 ATPase by accelerating ADP/ATP exchange. *Biochemistry* 31: 9406–9412. doi: [10.1021/bi00154a012](https://doi.org/10.1021/bi00154a012) PMID: [1356434](https://pubmed.ncbi.nlm.nih.gov/1356434/)
68. Huang SP, Tsai MY, Tzou YM, Wu WG, Wang C (1993) Aspartyl residue 10 is essential for ATPase activity of rat hsc70. *J Biol Chem* 268: 2063–2068. PMID: [8420978](https://pubmed.ncbi.nlm.nih.gov/8420978/)
69. Veyel D, Sommer F, Muranaka LS, Rtgers M, Lemaire SD, et al. (2014) In-vitro characterization of bacterial and chloroplast Hsp70 systems reveals an evolutionary optimization of the co-chaperones for their Hsp70 partner. *Biochem J* 460: 13–24. doi: [10.1042/BJ20140001](https://doi.org/10.1042/BJ20140001) PMID: [24564700](https://pubmed.ncbi.nlm.nih.gov/24564700/)
70. Lopez-Buesa P, Pfund C, Craig EA (1998) The biochemical properties of the ATPase activity of a 70-kDa heat shock protein (Hsp70) are governed by the C-terminal domains. *Proc Natl Acad Sci U S A* 95: 15253–15258. doi: [10.1073/pnas.95.26.15253](https://doi.org/10.1073/pnas.95.26.15253) PMID: [9860955](https://pubmed.ncbi.nlm.nih.gov/9860955/)
71. Araujo TLS, Borges JC, Ramos CHI, Meyer-Fernandes JR, Oliveira Junior RS, et al. (2014) Conformational changes in human Hsp70 induced by high hydrostatic pressure produce oligomers with ATPase activity but without chaperone activity. *Biochemistry* 53: 2884–2889. doi: [10.1021/bi500004q](https://doi.org/10.1021/bi500004q) PMID: [24739062](https://pubmed.ncbi.nlm.nih.gov/24739062/)